Computer Physics Communications 184 (2013) 2621–2633

Contents lists available at ScienceDirect

Computer Physics Communications

journal homepage: www.elsevier.com/locate/cpc

Feature article

Computational methods for the dynamics of the nonlinear Schrödinger/Gross–Pitaevskii equations

Xavier Antoine [a,b], Weizhu Bao [c,d,*], Christophe Besse [e,f]

[a] Université de Lorraine, Institut Elie Cartan de Lorraine, UMR 7502, Vandoeuvre-lès-Nancy, F-54506, France
[b] CNRS, Institut Elie Cartan de Lorraine, UMR 7502, Vandoeuvre-lès-Nancy, F-54506, France
[c] Department of Mathematics, National University of Singapore, Singapore 119076, Singapore
[d] Center for Computational Science and Engineering, National University of Singapore, Singapore 119076, Singapore
[e] Laboratoire Paul Painlevé, Université Lille Nord de France, CNRS UMR 8524, 59655 Villeneuve d'Ascq Cedex, France
[f] INRIA SIMPAF Team, Université Lille 1 Sciences et Technologies, Cité Scientifique, 59655 Villeneuve d'Ascq Cedex, France

ARTICLE INFO

Article history:
Received 26 April 2013
Received in revised form
10 July 2013
Accepted 13 July 2013
Available online 5 August 2013

Keywords:
Nonlinear Schrödinger equation
Gross–Pitaevskii equation
Time-splitting spectral method
Crank–Nicolson finite difference method
Absorbing boundary condition
Bose–Einstein condensation

ABSTRACT

In this paper, we begin with the nonlinear Schrödinger/Gross–Pitaevskii equation (NLSE/GPE) for modeling Bose–Einstein condensation (BEC) and nonlinear optics as well as other applications, and discuss their dynamical properties ranging from time reversible, time transverse invariant, mass and energy conservation, and dispersion relation to soliton solutions. Then, we review and compare different numerical methods for solving the NLSE/GPE including finite difference time domain methods and time-splitting spectral method, and discuss different absorbing boundary conditions. In addition, these numerical methods are extended to the NLSE/GPE with damping terms and/or an angular momentum rotation term as well as coupled NLSEs/GPEs. Finally, applications to simulate a quantized vortex lattice dynamics in a rotating BEC are reported.

1. Introduction

The nonlinear Schrödinger equation (NLSE) is a partial differential equation (PDE) that can be met in many different areas of physics and chemistry as well as engineering [1–7]. The most well-known and important derivation of the NLSE is from the mean-field approximation of many-body problems in quantum physics and chemistry [5], especially for the study of Bose–Einstein condensation (BEC) [5,8], where it is also called the Gross–Pitaevskii equation (GPE) [5,9–11]. Another important application of the NLSE is for laser beam propagation in nonlinear and/or quantum optics and there it is also known as parabolic/paraxial approximation of the Helmholtz or time-independent Maxwell equations [1–3,7]. Other important applications include long range wave propagation in underwater acoustics [7,12], plasma and particle physics [7], semiconductor industry [13,14], materials simulation based on the first principle [15], superfluids [16,17], and molecular systems in biology [18].

In this paper, we consider the following time-dependent NLSE [7,9]:

$$i\varepsilon\partial_t\psi(t,\mathbf{x}) = -\frac{\varepsilon^2}{2}\nabla^2\psi(t,\mathbf{x}) + V(\mathbf{x})\psi(t,\mathbf{x}) + f(|\psi(t,\mathbf{x})|^2)\psi(t,\mathbf{x}), \quad \mathbf{x}\in\mathbb{R}^d,\ t>0, \tag{1.1}$$

with initial data

$$\psi(t=0,\mathbf{x}) = \psi_0(\mathbf{x}), \quad \mathbf{x}\in\mathbb{R}^d, \tag{1.2}$$

where $i=\sqrt{-1}$ is the complex unit, t is the time variable, $\mathbf{x}\in\mathbb{R}^d$ is the spatial variable with $d=1,2,3$, $\psi := \psi(t,\mathbf{x})$ is the complex-valued wave function or order parameter, $\nabla^2 = \Delta$ is the usual Laplace operator and $\psi_0 := \psi_0(\mathbf{x})$ is a given complex-valued initial data. Moreover, $0<\varepsilon\leq 1$ is a dimensionless parameter. In most physics literatures, it is taken equal to $\varepsilon=1$; however in the semiclassical regime, we have $0<\varepsilon\ll 1$, ε being also called the "scaled" Planck constant. Function $V := V(\mathbf{x})$ is a given real-valued external potential and its specific form depends on different applications and could also sometimes be time dependent [5,7,9,19]. For example, in BEC, it is usually chosen as either a harmonic confining

* Corresponding author at: Department of Mathematics, National University of Singapore, Singapore 119076, Singapore. Tel.: +65 6516 2765; fax: +65 6779 5452.
E-mail addresses: xavier.antoine@univ-lorraine.fr (X. Antoine), matbaowz@nus.edu.sg, bao@math.nus.edu.sg (W. Bao), christophe.besse@math.univ-lille1.fr (C. Besse).
URL: http://www.math.nus.edu.sg/~bao/ (W. Bao).

0010-4655/$ – see front matter © 2013 Elsevier B.V. All rights reserved.
http://dx.doi.org/10.1016/j.cpc.2013.07.012

potential, i.e. $V(\mathbf{x}) = \frac{|\mathbf{x}|^2}{2}$ [5,9,19], or an optical lattice potential, i.e. $V(\mathbf{x}) = A_1\cos(L_1x) + A_2\cos(L_2y) + A_3\cos(L_3z)$, in three dimensions (3D) with A_1, A_2, A_3, L_1, L_2 and L_3 constants [5,9,19–21], or a stochastic potential for producing speckle patterns [5,22]; in nonlinear optics, it might be chosen as an attractive potential, i.e. $V(\mathbf{x}) = -\frac{|\mathbf{x}|^2}{2}$ [1,3]. The nonlinearity $f := f(\rho)$ is a real-valued smooth function depending on the density $\rho := |\psi|^2 \in [0, \infty)$ and its specific form depends on different applications [1,2,5,7,9,19]. In fact, when $f(\rho) \equiv \lambda$, with λ a constant, then the NLSE (1.1) collapses to the standard (linear) Schrödinger equation [4,6]. The most popular and important nonlinearity is the cubic nonlinearity [1,2,5,7,9]:

$$f(\rho) = \beta\rho, \quad 0 \le \rho < \infty, \tag{1.3}$$

where β (positive for the repulsive or defocusing interaction and negative for the attractive or focusing interaction) is a given dimensionless constant describing the strength of interaction. Other nonlinearities used in nonlinear optics include the cubic–quintic nonlinearity $f(\rho) = \beta_1\rho + \beta_2\rho^2$ [1,3,7,12] and the saturation of the intensity nonlinearity $f(\rho) = \frac{\beta_0\rho}{1+c_0\rho}$ with $\beta_0, \beta_1, \beta_2$ and c_0 given constants [1,3,7,12]. In some applications, nonlocal nonlinearities can also be considered, and in this case $f(\rho) = U * \rho$ which is a convolution, with $U := U(\mathbf{x})$ the kernel [9,23–27]. Specifically, for the Hartree potential case, $U(\mathbf{x}) = \frac{1}{4\pi|\mathbf{x}|}$ is Green's function of the Laplace operator in 3D, and then, the NLSE (1.1) can be re-written as the Schrödinger–Poisson system in 3D [25,28]. Finally, we remark here that the NLSE (1.1) is also called the Gross–Pitaevskii Equation (GPE) when the nonlinearity is chosen as the cubic nonlinearity as in (1.3), especially in BEC [5,9,19]. Thus GPE is a special version of NLSE [5,9–11,19].

There are many important dynamical properties of the solution ψ to the NLSE (1.1). Among them, here we mention several important ones that we will use to justify different numerical methods on whether they are still valid at the discrete level after the NLSE (1.1) is discretized by a numerical method. In fact, the NLSE (1.1) is a dispersive PDE and it is *time reversible or symmetric*, i.e. it is unchanged under the change of variable in time as $t \to -t$ and taken conjugate in the equation. Another important property is *time transverse or gauge invariant*, i.e. if $V \to V + \alpha$, with α a given real constant, then the solution $\psi \to \psi e^{-i\alpha t/\varepsilon}$ which immediately implies that the density $\rho = |\psi|^2$ is unchanged. The NLSE (1.1) conserves many quantities. Among them, the *mass* (or wave energy in nonlinear optics) and *energy* (or Hamiltonian in nonlinear optics) *conservation* are given as [7,9,29]

$$\begin{aligned} N(t) &:= \|\psi(t,\cdot)\|^2 = \int_{\mathbb{R}^d} |\psi(t,\mathbf{x})|^2 d\mathbf{x} \equiv \int_{\mathbb{R}^d} |\psi(0,\mathbf{x})|^2 d\mathbf{x} \\ &= \int_{\mathbb{R}^d} |\psi_0(\mathbf{x})|^2 d\mathbf{x} := N(0), \quad t \ge 0, \end{aligned} \tag{1.4}$$

$$\begin{aligned} E(t) &:= \int_{\mathbb{R}^d} \left[\frac{\varepsilon^2}{2} |\nabla\psi(t,\mathbf{x})|^2 + V(\mathbf{x})|\psi(t,\mathbf{x})|^2 \right. \\ &\quad \left. + F(|\psi(t,\mathbf{x})|^2) \right] d\mathbf{x} \equiv E(0), \quad t \ge 0, \end{aligned} \tag{1.5}$$

respectively, with

$$F(\rho) := \int_0^\rho f(s)\, ds, \quad 0 \le \rho < +\infty. \tag{1.6}$$

If there is no external potential in the NLSE (1.1), i.e. $V(\mathbf{x}) \equiv 0$, then the momentum and angular momentum are also conserved [7,9,29]. In addition, the NLSE (1.1) admits the plane wave solution as $\psi(t,\mathbf{x}) = Ae^{i(\mathbf{k}\cdot\mathbf{x}-\omega t)}$, where the time frequency ω, amplitude A and spatial wave number $\mathbf{k}$ satisfy the following *dispersion relation* [7,9,29,30]

$$\omega = \frac{\varepsilon|\mathbf{k}|^2}{2} + \frac{1}{\varepsilon} f(|A|^2). \tag{1.7}$$

In this case, if in 1D with $\varepsilon = 1$ and the nonlinearity is chosen as the focusing cubic nonlinearity (1.3) with $\beta < 0$, it also admits the well-known bright soliton solution as [1–3,7,12,31]

$$\begin{aligned} \psi_B(t,x) &= \frac{A}{\sqrt{-\beta}} \operatorname{sech}(A(x - vt - x_0)) e^{i\left(vx - \frac{1}{2}(v^2 - A^2)t + \theta_0\right)}, \\ x &\in \mathbb{R}, \ t \ge 0, \end{aligned} \tag{1.8}$$

where $\frac{A}{\sqrt{-\beta}}$ is the amplitude of the soliton with A a real constant, v is the velocity of the soliton, x_0 and θ_0 are the initial shifts in space and phase, respectively. Since the soliton solution is exponentially decaying for $|x| \to +\infty$, then the mass and energy are well defined and given by $N(\psi_B) = -\frac{2A}{\beta}$ and $E(\psi_B) = \frac{Av^2}{-\beta} + \frac{A^3}{-3\beta}$. For other more dynamical properties of the NLSE (1.1) such as dark (black and gray) solitons in 1D under defocusing cubic nonlinearity, well-posedness and finite time blow-up, we refer the reader to [9,7,29,32,33] and references therein.

For studying numerically the dynamics of the NLSE (1.1), different numerical methods have been proposed in the literatures [9,19,34–51] and references therein. The main aim of this paper is to review different numerical methods for solving the NLSE (1.1) numerically, compare them in terms of keeping different dynamical properties at the discretized level, stability and accuracy, discuss different absorbing boundary conditions for truncating the NLSE (1.1) onto a bounded computational domain, and extend them for solving NLSE with damping and/or angular momentum terms as well as coupled NLSEs.

The paper is organized as follows. In Section 2, we review several popular numerical methods in the literatures for discretizing the NLSE/GPE under simple boundary conditions and compare their advantages and disadvantages, discuss different absorbing boundary conditions for the NLSE/GPE, and review some robust and efficient numerical methods for the NLSE/GPE in the semi-classical regime. Extensions to the NLSE/GPE with damping and/or angular rotating terms and coupled NLSEs/GPEs are presented in Sections 3 and 4, respectively. The numerical comparison of different numerical methods and some applications are reported in Section 5. Finally, we draw some conclusions and discuss future perspectives in Section 6.

2. Numerical methods for the NLSE/GPE

2.1. Some popular numerical methods

Here we present several popular numerical methods for discretizing the NLSE/GPE (1.1) and discuss/compare their properties including stability, accuracy, computational cost and how much properties of the NLSE/GPE that these numerical methods can keep at the discretized level. For simplicity of notation, we shall introduce these methods in one space dimension (1D), i.e. $d = 1$ in (1.1). Generalizations to $d > 1$ are straightforward for tensor product grids and the results remain valid with modifications. For $d = 1$, the NLSE/GPE (1.1) truncated on a bounded interval (a, b) with the homogeneous Dirichlet boundary condition ($|a|$ and b large enough so that the error due to the truncation is negligible) becomes

$$\begin{aligned} i\varepsilon\partial_t\psi(t,x) &= -\frac{\varepsilon^2}{2}\partial_{xx}\psi(t,x) + V(x)\psi(t,x) \\ &\quad + f(|\psi(t,x)|^2)\psi(t,x), \quad a < x < b, \ t > 0, \end{aligned} \tag{2.1}$$

$$\psi(t,a) = \psi(t,b) = 0, \quad t \ge 0, \tag{2.2}$$

$$\psi(t=0,x) = \psi_0(x), \quad a \le x \le b. \tag{2.3}$$

In this case, the *mass* and *energy conservation* collapse to the following:

$$N(t) := \|\psi(t,\cdot)\|^2 = \int_a^b |\psi(t,x)|^2 dx \equiv \int_a^b |\psi(0,x)|^2 dx = \int_a^b |\psi_0(x)|^2 dx := N(0), \quad t \geq 0, \tag{2.4}$$

$$E(t) := \int_a^b \left[\frac{\varepsilon^2}{2}|\partial_x \psi(t,x)|^2 + V(x)|\psi(t,x)|^2 + F(|\psi(t,x)|^2)\right] dx \equiv E(0), \quad t \geq 0. \tag{2.5}$$

Choose a time step $\tau := \Delta t > 0$ and denote the different times as $t_n := n\tau$ for $n = 0, 1, 2, \ldots$; choose the mesh size $h := \Delta x = \frac{b-a}{J}$, with J an even positive integer, and denote the grid points by $x_j := a + jh$, for $j = 0, 1, \ldots, J$. Let ψ_j^n be the numerical approximation of $\psi(t_n, x_j)$, for $j = 0, 1, \ldots, J$ and $n = 0, 1, 2, \ldots$; let $\boldsymbol{\psi}^n$ be the solution vector at time $t = t_n$ with components $(\psi_j^n)_{0\leq j\leq J}$. In addition, for any complex-valued vector $\boldsymbol{\phi} = (\phi_j)_{0\leq j\leq J}$, we define the following finite difference operators:

$$(D_x^+ \boldsymbol{\phi})_j = \frac{\phi_{j+1} - \phi_j}{h}, \quad 0 \leq j \leq J-1; \qquad (D_x^2 \boldsymbol{\phi})_j = \frac{\phi_{j+1} - 2\phi_j + \phi_{j-1}}{h^2}, \quad 1 \leq j \leq J-1. \tag{2.6}$$

Then the *Crank–Nicolson finite difference* (CNFD) method – in which one applies the second-order centered difference scheme for spatial discretization and the Crank–Nicolson scheme for time discretization – for discretizing (2.1) reads as [9,45,52–56]

$$i\varepsilon \frac{\psi_j^{n+1} - \psi_j^n}{\tau} = -\frac{\varepsilon^2}{4}\left[\left(D_x^2 \boldsymbol{\psi}^{n+1}\right)_j + \left(D_x^2 \boldsymbol{\psi}^n\right)_j\right] + \left[V(x_j) + G\left(|\psi_j^{n+1}|^2, |\psi_j^n|^2\right)\right] \frac{\psi_j^{n+1} + \psi_j^n}{2}, \quad 1 \leq j \leq J-1, \ n \geq 0, \tag{2.7}$$

where

$$G(\rho_1, \rho_2) = \frac{F(\rho_1) - F(\rho_2)}{\rho_1 - \rho_2} := \int_0^1 f(\theta\rho_1 + (1-\theta)\rho_2)\, d\theta, \quad 0 \leq \rho_1, \rho_2 < \infty.$$

The boundary and initial conditions (2.2)–(2.3) are discretized as

$$\psi_0^{n+1} = \psi_J^{n+1} = 0, \quad n \geq 0; \qquad \psi_j^0 = \psi_0(x_j), \quad 0 \leq j \leq J. \tag{2.8}$$

The above CNFD method (2.7) is *time reversible or symmetric*, i.e. it is unchanged if $\tau \to -\tau$ and $n+1 \leftrightarrow n$, and its memory cost is $\mathcal{O}(J^d)$ in d-dimensions with J unknowns in each direction. It conserves the *mass* (2.4) and *energy* (2.5) in the discretized level [9,52,54,55,57], i.e.

$$N^n := h\sum_{j=1}^{J-1} |\psi_j^n|^2 \equiv h\sum_{j=1}^{J-1} |\psi_j^0|^2 = h\sum_{j=1}^{J-1} |\psi_0(x_j)|^2 := N^0, \quad n \geq 0, \tag{2.9}$$

$$E^n := h\sum_{j=0}^{J-1}\left[\frac{\varepsilon^2}{2}\left|\left(D_x^+ \boldsymbol{\psi}^n\right)_j\right|^2 + V(x_j)|\psi_j^n|^2 + F(|\psi_j^n|^2)\right] \equiv E^0, \quad n \geq 0, \tag{2.10}$$

which immediately implies that the CNFD method is unconditionally stable. In addition, it can be proven rigorously in mathematics that the CNFD method is second-order accurate in both time and space for any fixed $\varepsilon = \varepsilon_0 = \mathcal{O}(1)$ [9,52,54,55,57]. However, it cannot preserve the *time transverse invariant* and *dispersion relation* properties of the NLSE/GPE (2.1) at the discretized level [9,52,57]. Furthermore, it is an implicit scheme and its practical implementation is a little tedious. In fact, at each time step, one needs to solve a coupled fully nonlinear system which can be solved by a fixed point or a modified Newton–Raphson iterative method [9,34,52,57–59] and thus it might be very time consuming. In general, the computational cost per time step is much larger than $\mathcal{O}(J^d)$, especially in 2D and 3D. In fact, if the nonlinear system in (2.7) is not solved very accurately, e.g. up to machine precision, the numerical solution computed from (2.7) does not conserve the energy in (2.10) *exactly* [57].

Due to the high computational cost of the CNFD method, in the literatures it is motivated for considering some semi-implicit methods in which a linear system is to be solved at every time step. Thus, the computational cost is significantly reduced, especially in 2D and 3D. One of these numerical methods is the *relaxation finite difference* (ReFD) method – in which one gives a name to the nonlinear term and makes a second-order approximation at time t_n – for the NLSE (2.1) [39]

$$\begin{cases} \dfrac{1}{2}\left(u_j^{n+1/2} + u_j^{n-1/2}\right) = f(|\psi_j^n|^2), \quad 1 \leq j \leq J-1, \ n \geq 0, \\ i\varepsilon \dfrac{\psi_j^{n+1} - \psi_j^n}{\tau} = -\dfrac{\varepsilon^2}{4}\left[\left(D_x^2 \boldsymbol{\psi}^{n+1}\right)_j + \left(D_x^2 \boldsymbol{\psi}^n\right)_j\right] \\ \qquad + \dfrac{1}{2}\left[V(x_j) + u_j^{n+1/2}\right]\left(\psi_j^{n+1} + \psi_j^n\right), \end{cases} \tag{2.11}$$

where $u_j^{-1/2} = \psi_j^0 = \psi_0(x_j)$ for $0 \leq j \leq J$. The boundary and initial conditions (2.2)–(2.3) are discretized as (2.8). Similarly, this ReFD method is *time reversible or symmetric*, its memory cost is $\mathcal{O}(J^d)$ in d-dimensions with J unknowns in each direction, and it is easier to be implemented than that of CNFD. It is an implicit scheme where, at each time step, only a linear system needs to be solved for example by the Thomas algorithm at the cost of $\mathcal{O}(J)$ in 1D and by some iterative methods such as the conjugate gradient (CG) or multigrid (MG) method [39,60] in 2D and 3D at the cost, in general, larger than $\mathcal{O}(J^d)$. Thus it is computationally much cheaper than that of the CNFD method. It conserves the *mass* (1.4) at the discretized level as (2.9) [39], and thus it is unconditionally stable. In addition, it can be mathematically proven rigorously that the ReFD method is second-order accurate in both time and space for any fixed $\varepsilon = \varepsilon_0 = \mathcal{O}(1)$ [39]. Furthermore, for the NLSE with the cubic nonlinearity (1.3), this method also conserves the following discrete energy defined as

$$\tilde{E}^n := h\sum_{j=0}^{J-1}\frac{\varepsilon^2}{2}\left|\left(D_x^+ \boldsymbol{\psi}^n\right)_j\right|^2 + h\sum_{j=1}^{J-1}\left[V(x_j)|\psi_j^n|^2 + \frac{\beta}{2}u_j^{n+1/2}u_j^{n-1/2}\right] \equiv \tilde{E}^0, \quad n \geq 0. \tag{2.12}$$

Of course, it cannot preserve the *time transverse invariant* and *dispersion relation* properties of the NLSE/GPE (2.1) in the discretized level [39]. In addition, for general nonlinearity other than the cubic nonlinearity, no discrete energy conservation has been proven for the ReFD method yet. Another popular method is the following *semi-implicit finite difference* (SIFD) method – in which one uses the

leap-frog scheme for the nonlinear term in time discretization – for the NLSE (2.1) [9,52,57]

$$i\varepsilon\frac{\psi_j^{n+1}-\psi_j^{n-1}}{2\tau} = -\frac{\varepsilon^2}{4}\left[\left(D_x^2\boldsymbol{\psi}^{n+1}\right)_j+\left(D_x^2\boldsymbol{\psi}^{n-1}\right)_j\right] + \left[V(x_j)+f(|\psi_j^n|^2)\right]\psi_j^n, \quad 1\le j\le J-1,\ n\ge 1; \tag{2.13}$$

or

$$i\varepsilon\frac{\psi_j^{n+1}-\psi_j^{n-1}}{2\tau} = -\frac{\varepsilon^2}{4}\left[\left(D_x^2\boldsymbol{\psi}^{n+1}\right)_j+\left(D_x^2\boldsymbol{\psi}^{n-1}\right)_j\right] + V(x_j)\frac{\psi_j^{n+1}+\psi_j^n}{2}+f(|\psi_j^n|^2)\psi_j^n, \quad 1\le j\le J-1,\ n\ge 1. \tag{2.14}$$

The boundary and initial conditions (2.2)–(2.3) are discretized as (2.8) and the first step can be computed as [9,52,57]

$$\psi_j^1=\psi_j^0-\frac{i\tau}{\varepsilon}\left[-\frac{\varepsilon^2}{2}\left(D_x^2\boldsymbol{\psi}^0\right)_j+V(x_j)\psi_j^0+f(|\psi_j^0|^2)\psi_j^0\right], \quad 1\le j\le J-1. \tag{2.15}$$

Again, this SIFD method is *time reversible or symmetric*, i.e. it is unchanged if $\tau\to-\tau$ and $n+1\leftrightarrow n-1$; its memory cost is $\mathcal{O}(J^d)$ in d-dimensions considering J unknowns in each direction. It is also much easier to be implemented than that of CNFD and ReFD, especially in 2D and 3D. It is an implicit scheme where, at each time step, only a linear system (whose coefficient matrix is time independent) needs to be solved, by the Thomas algorithm in $\mathcal{O}(J)$ operations in 1D and by the direct fast Poisson solver *via* the discrete sine transform (DST) at the cost of $\mathcal{O}(J^d\ln J)$ in 2D and 3D. Thus, it is significantly cheaper than the CNFD and ReFD methods, especially in 2D/3D. In addition, it can be proven that the SIFD method is second-order accurate both in time and space for any fixed $\varepsilon=\varepsilon_0=\mathcal{O}(1)$ [9,52,57] and a fourth-order (or six-order or even eighth-order) accurate method can be very easily constructed *via* the Richardson extrapolation technique [61]. Of course, it is conditionally stable under the stability condition $\tau\lesssim\tau_n:=\frac{1}{\varepsilon\max_{0\le j\le J}|V(x_j)+f(|\psi_j^n|^2)|}$ (or $\tau\lesssim\tau_n:=\frac{1}{\varepsilon\max_{0\le j\le J}|f(|\psi_j^n|^2)|}$ for (2.14)) for $n\ge 0$, which is independent of the mesh size h. It cannot preserve the *time transverse invariant*, *dispersion relation* and *mass* and *energy conservation* properties of the NLSE/GPE (2.1) in the discretized level [9,52,57].

Another way to handle the nonlinearity in (2.1) is to use the time-splitting technique [9,20,21,36–38,46,49–51,62–64], i.e. from time $t=t_n$ to time $t=t_{n+1}$, Eq. (2.1) is solved in two splitting steps. One solves first

$$i\varepsilon\partial_t\psi(t,x)=-\frac{\varepsilon^2}{2}\partial_{xx}\psi(t,x), \quad a<x<b,\ t>t_n, \tag{2.16}$$

with the homogeneous Dirichlet boundary condition (2.2) for the time step of length τ, followed by solving

$$i\varepsilon\partial_t\psi(t,x)=V(x)\psi(t,x)+f(|\psi(t,x)|^2)\psi(t,x), \quad a\le x\le b,\ t>t_n, \tag{2.17}$$

for the same time step. Eq. (2.16) will be first discretized in space by the sine spectral method and then integrated (in phase space) in time *exactly* [9,36–38,65]. Multiplying (2.17) by $\overline{\psi(t,x)}$ (conjugate of $\psi(t,x)$) and then subtracting from its conjugate [9,36–38], we get for $\rho(t,x):=|\psi(t,x)|^2$

$$\partial_t\rho(t,x)=0, \quad t>t_n,\ a\le x\le b, \tag{2.18}$$

which immediately implies that the density ρ is invariant for any fixed x in the second splitting step (2.17), i.e.

$$\rho(t,x):=|\psi(t,x)|^2 \equiv |\psi(t_n,x)|^2=\rho(t_n,x), \quad t\ge t_n,\ a\le x\le b. \tag{2.19}$$

Plugging (2.19) into (2.17), Eq. (2.17) collapses to a linear ODE as

$$i\varepsilon\partial_t\psi(t,x)=V(x)\psi(t,x)+f(|\psi(t_n,x)|^2)\psi(t,x), \quad a\le x\le b,\ t>t_n, \tag{2.20}$$

which can be integrated *analytically* as

$$\psi(t,x)=e^{-i\left[V(x)+f(|\psi(t_n,x)|^2)\right](t-t_n)/\varepsilon}\psi(t_n,x), \quad t\ge t_n,\ a\le x\le b. \tag{2.21}$$

In practical computation, from time $t=t_n$ to $t=t_{n+1}$, one often combines the splitting steps *via* the standard Strang splitting [66] – which is usually referred to as time-splitting sine pseudospectral (TSSP) method [9,36–38,65] – as

$$\begin{aligned}\psi_j^{(1)}&=e^{-i\tau[V(x_j)+f(|\psi_j^n|^2)]/2\varepsilon}\psi_j^n,\\ \psi_j^{(2)}&=\sum_{l=1}^{J-1}e^{-i\tau\,\varepsilon\,\mu_l^2/2}(\widehat{\psi^{(1)}})_l\sin\left(\mu_l(x_j-a)\right)\\ &=\sum_{l=1}^{J-1}e^{-i\tau\,\varepsilon\,\mu_l^2/2}(\widehat{\psi^{(1)}})_l\sin\left(\frac{lj\pi}{J}\right),\\ \psi_j^{n+1}&=e^{-i\tau[V(x_j)+f(|\psi_j^{(2)}|^2)]/2\varepsilon}\psi_j^{(2)}, \quad 1\le j\le J-1,\ n\ge 0,\end{aligned} \tag{2.22}$$

where $\psi_0^{n+1}=\psi_J^{n+1}=0$ for $n\ge 0$, $\psi_j^0=\psi_0(x_j)$ for $0\le j\le J$, and $(\widehat{\psi^{(1)}})_l$ for $1\le l\le J-1$, the discrete sine transform coefficients of the complex-valued vector $\psi^{(1)}=(\psi_0^{(1)},\psi_1^{(1)},\dots,\psi_J^{(1)})^T$ with $\psi_0^{(1)}=\psi_J^{(1)}=0$, are defined by

$$\begin{aligned}\mu_l&=\frac{\pi l}{b-a},\\ \widehat{\psi}_l^{(1)}&=\frac{2}{J}\sum_{j=1}^{J-1}\psi_j^{(1)}\sin\left(\mu_l(x_j-a)\right)\\ &=\frac{2}{J}\sum_{j=1}^{J-1}\psi_j^{(1)}\sin\left(\frac{lj\pi}{J}\right), \quad 1\le l\le J-1.\end{aligned} \tag{2.23}$$

Again, the above TSSP method is *time reversible or symmetric*, its memory cost is $\mathcal{O}(J^d)$ in d-dimensions with J unknowns along each direction. Its implementation is much easier than for CNFD, ReFD and SIFD. It is an explicit scheme since there is no need to solve a linear system and, at each time step, the computational cost is $\mathcal{O}(J^d\ln J)$. It conserves the *mass* (2.4) in the discretized level as (2.9) [9,36–38,65], and it is therefore unconditionally stable. In addition, it can be rigorously proven that the TSSP method is second-order accurate in time and spectral order accurate in space for any fixed $\varepsilon=\varepsilon_0=\mathcal{O}(1)$ [9,67–72]. In addition, it is *time transverse invariant*, i.e. when $V(x)\to V(x)+\alpha$ with α a constant, then $\psi_j^n\to\psi_j^n e^{-i\alpha n\tau/\varepsilon}$ which implies that the density $\rho_j^n:=|\psi_j^n|^2$ is unchanged; it has the same *dispersion relation* as the NLSE/GPE (2.1), i.e. if $V(x)\equiv 0$ and $\psi_0(x_j)=Ae^{ikx_j}$ for $0\le j\le J$, then the numerical solution from the TSSP method is $\psi_j^n=Ae^{i(kx_j-\omega t_n)}$ with ω, A and k satisfying the dispersion relation (1.7) provided that $J\ge k$ and the sine basis is replaced by the Fourier basis in the TSSP method [36–38]. However, it cannot preserve *energy conservation* properties of the NLSE/GPE (2.1) in the discretized level [37,38]. In fact, the numerical solution from the TSSP method actually coincides with the exact solution of a modified PDE at each time step. This shows the existence of a modified energy [73–77]

Table 1
Physical and numerical properties of different popular numerical methods in the d-dimensional case with J unknowns in each direction.

Method	TSSP	CNFD	SIFD	ReFD	TSFD
Time reversible	Yes	Yes	Yes	Yes	Yes
Time transverse invariant	Yes	No	No	No	Yes
Mass conservation	Yes	Yes	No	Yes	Yes
Energy conservation	No	Yes	No	Yes[a]	No
Dispersion relation	Yes	No	No	No	Yes
Unconditional stability	Yes	Yes	No	Yes	Yes
Explicit scheme	Yes	No	No	No	No
Time accuracy	2nd or 4th	2nd	2nd	2nd	2nd
Spatial accuracy	Spectral	2nd	2nd	2nd	2nd
Memory cost	$\mathcal{O}(J^d)$	$\mathcal{O}(J^d)$	$\mathcal{O}(J^d)$	$\mathcal{O}(J^d)$	$\mathcal{O}(J^d)$
Computational cost	$\mathcal{O}(J^d \log J)$	$\gg\mathcal{O}(J^d)$[b]	$\mathcal{O}(J^d \log J)$[c]	$\mathcal{O}(J^d \log J)$[d]	$\mathcal{O}(J^d \log J)$[e]
Resolution when $0<\varepsilon\ll 1$[f]	$h=\mathcal{O}(\varepsilon)$ $\tau=\mathcal{O}(\varepsilon)$	$h=o(\varepsilon)$ $\tau=o(\varepsilon)$	$h=o(\varepsilon)$ $\tau=o(\varepsilon)$	$h=o(\varepsilon)$ $\tau=o(\varepsilon)$	$h=o(\varepsilon)$ $\tau=o(\varepsilon)$

[a] Only for cubic nonlinearity.
[b] Depends on the solver for the nonlinear system.
[c] If $d=1$, $\mathcal{O}(J)$.
[d] If $d=1$, $\mathcal{O}(J)$.
[e] If $d=1$, $\mathcal{O}(J)$.
[f] For cubic repulsive nonlinearity.

preserved by the numerical scheme that is close to the exact energy if the numerical solution is smooth. However, some resonances may destroy the energy conservation on long time evolution (see Chapter 7 of [76]). Finally, for designing high-order, e.g. fourth-order accurate in time, time-splitting spectral methods, we refer the reader to [62,64,65,72,78,79] and references therein.

In the literatures, in some applications where the solution of the NLSE/GPE is not smooth, e.g. with random potential [22, 80–82], then the following time-splitting finite difference (TSFD) – in which the time-splitting is applied first and then the free Schrödinger equation (2.16) is discretized by the CNFD method – is used for discretizing the NLSE/GPE [9,31,83,84] as

$$\begin{aligned}
&\psi_j^{(1)} = e^{-i\tau[V(x_j)+f(|\psi_j^n|^2)]/2\varepsilon}\psi_j^n, \quad 0\le j\le J,\\
&i\varepsilon\frac{\psi_j^{(2)}-\psi_j^{(1)}}{\tau} = -\frac{\varepsilon^2}{4}\left[\left(D_x^2\boldsymbol{\psi}^{(2)}\right)_j+\left(D_x^2\boldsymbol{\psi}^{(1)}\right)_j\right],\\
&\quad 1\le j\le J-1, \qquad \psi_0^{(2)}=\psi_J^{(2)}=0,\\
&\psi_j^{n+1} = e^{-i\tau[V(x_j)+f(|\psi_j^{(2)}|^2)]/2\varepsilon}\psi_j^{(2)}, \quad 0\le j\le J,\ n\ge 0,
\end{aligned} \tag{2.24}$$

where $\psi_j^0=\psi_0(x_j)$ for $0\le j\le J$. Similarly, the above TSFD method is *time reversible or symmetric*, its memory cost is $\mathcal{O}(J^d)$ in d-dimensions with J unknowns in each direction; it is easier to be implemented than CNFD, ReFD and SIFD. It is an implicit scheme where, at each time step, only a linear system (whose coefficient matrix is time independent) needs to be solved, which can be done in $\mathcal{O}(J)$ operations in 1D and $\mathcal{O}(J^d \ln J)$ operations in 2D/3D. Therefore it is significantly cheaper than the CNFD and ReFD methods. The TSFD method is second-order accurate both in time and space for any fixed $\varepsilon=\varepsilon_0=\mathcal{O}(1)$ [9,31]. In addition, it conserves the *mass* (2.4) at the discretized level as (2.9) [9,31,83] and thus it is unconditionally stable; it is also *time transverse invariant*. However, there is no *energy conservation* property of the NLSE/GPE (2.1) at the discretized level [9,31,83].

For comparison and convenience of the readers, we summarize the main physical and computational properties of the above popular numerical methods CNFD, ReFD, SIFD, TSSP and TSFD in Table 1. From this table, we can see that the TSSP method shares the most properties as the original NLSE/GPE. In addition, it is very efficient and accurate as well as easy to be implemented in practical computations, especially in 2D and 3D [9,36–38,62,64]. In fact, the TSSP method becomes more and more popular in practical computations, especially in the numerical simulation of Bose–Einstein condensation [9,20,21,36,62,64,85].

Remark 2.1. If the homogeneous Dirichlet boundary condition (2.2) is replaced by the periodic boundary condition, e.g. for BEC on a ring [9,31,37,38], the above numerical methods are still valid provided that we replace $1\le j\le J-1$ by $0\le j\le J-1$ in all the numerical methods, and replace $\psi_0^{n+1}=\psi_J^{n+1}=0$ by $\psi_0^{n+1}=\psi_J^{n+1}$ and $\psi_{-1}^{n+1}=\psi_{J-1}^{n+1}$ in the CNFD, ReFD and SIFD methods, the sine basis by the Fourier basis in the TSSP method, and $\psi_0^{(2)}=\psi_J^{(2)}=0$ by $\psi_0^{(2)}=\psi_J^{(2)}$ and $\psi_{-1}^{(2)}=\psi_{J-1}^{(2)}$ in the TSFD method, respectively. Similarly, if the homogeneous Dirichlet boundary condition (2.2) is replaced by the homogeneous Neumann boundary condition, e.g. for the dynamics of dark solitons and their interaction [9,31,86], the above numerical methods are still valid provided that we replace $1\le j\le J-1$ by $0\le j\le J$ in all the numerical methods, and replace $\psi_0^{n+1}=\psi_J^{n+1}=0$ by $\psi_{-1}^{n+1}=\psi_0^{n+1}$ and $\psi_{J+1}^{n+1}=\psi_{J-1}^{n+1}$ in the CNFD, ReFD and SIFD methods, the sine basis by the cosine basis in the TSSP method, and $\psi_0^{(2)}=\psi_J^{(2)}=0$ by $\psi_{-1}^{(2)}=\psi_0^{(2)}$ and $\psi_{J+1}^{(2)}=\psi_{J-1}^{(2)}$ in the TSFD method, respectively [9,31,86]. Then the physical and numerical properties of these numerical methods are still valid.

2.2. Other numerical methods

In the literatures, there are many other numerical methods proposed for discretizing the NLSE/GPE. For example, Sanz-Serna [44,87–89] proposed the following second-order finite difference (SSFD) method which is well-adapted to the computation of soliton-like solutions of the NLSE/GPE

$$\begin{aligned}
i\varepsilon\frac{\psi_j^{n+1}-\psi_j^n}{\tau} &= -\frac{\varepsilon^2}{4}\left[\left(D_x^2\boldsymbol{\psi}^{n+1}\right)_j+\left(D_x^2\boldsymbol{\psi}^n\right)_j\right]\\
&\quad+\left[V(x_j)+f\left(\left|\frac{\psi_j^{n+1}+\psi_j^n}{2}\right|^2\right)\right]\frac{\psi_j^{n+1}+\psi_j^n}{2},\\
&\quad 1\le j\le J-1,\ n\ge 0,
\end{aligned} \tag{2.25}$$

and the boundary and initial conditions (2.2)–(2.3) are discretized as (2.8). Another one is the leap-frog finite difference (LPFD) method as [90,91]

$$\begin{aligned}
&i\varepsilon\frac{\psi_j^{n+1}-\psi_j^{n-1}}{2\tau} = -\frac{\varepsilon^2}{2}\left(D_x^2\boldsymbol{\psi}^n\right)_j+\left[V(x_j)+f\left(\left|\psi_j^n\right|^2\right)\right]\psi_j^n,\\
&\quad 1\le j\le J-1, \quad n\ge 1,
\end{aligned} \tag{2.26}$$

and the boundary and initial conditions (2.2)–(2.3) are discretized as (2.8) and the first step can be computed as (2.15). In fact, in the physics literatures, for time discretization, the fourth-order Runge–Kutta (RK4) method was also used [92–95], which is not time symmetric. Thus, in general, it should be avoided to use RK4 for solving the NLSE/GPE. In some mathematics literatures, for space discretization, the 4th-order compact finite difference method has been used [96,97,61] and the finite element (FE) method was also developed and analyzed [34,59]. However, since the computational domains for the NLSE/GPE are usually simple and regular, the FE method for spatial discretization is usually not adapted in practical computations. Last but not the least, we want to mention that, in some physics papers, for solving the NLSE/GPE in 2D or 3D, the alternating direction implicit (ADI) is first adapted to decouple the NLSE/GPE into dimension-by-dimension and then the SIFD or CNFD is used to discretize each NLSE/GPE in 1D [90,92,98–101]. For other more numerical methods for the NLSE/GPE, we refer the reader to [30,40–43,58,86,87,90,93,100,102–116] and references therein. In general, these numerical methods have less good properties as those methods mentioned in the previous subsection and thus we omit the details here for brevity.

2.3. Perfectly matched layers and/or absorbing boundary conditions

In some situations for solving the NLSE/GPE (1.1) numerically, e.g. very long time dynamics and the potential is not a confinement potential in nonlinear optics [117,118], the simple boundary condition, such as homogeneous Dirichlet or Neumann or periodic boundary condition used in the previous subsections to truncate (or approximate) the original NLSE/GPE from the whole space problem to a bounded computational domain, might bring large truncation errors except that the bounded computational domain is chosen extremely large and/or time-dependent. Thus, in order to choose a smaller computational domain which might save memory and/or computational cost, perfectly matched layers (PMLs) [119] or high-order absorbing (or artificial) boundary conditions (ABCs) [35,117,118,120–123] need to be designed and/or used at the artificial boundary so that one can truncate (or approximate) the original NLSE/GPE into a smaller bounded computational domain. Over the last 20 years, different PMLs [124,125] and/or ABCs [117,118,126–134] have been designed for solving the NLSE/GPE in the literatures. Here we simply review some of them for the completeness of this paper.

In fact, PMLs were introduced by Bérenger in 1994 for electromagnetic field computations [119] and they have been extended to the NLSE/GPE by various authors recently [124,125]. Again, here we present the idea in 1D. Suppose that one is only interested in the solution of the NLSE/GPE (1.1) with $d = 1$ over the physical domain (a, b). One introduces two layers with width $R_0 > 0$ at $x = a$ and $x = b$ and defines the following function:

$$S(x) := 1 + R\sigma(x), \qquad \tilde{a} := a - R_0 \le x \le b + R_0 := \tilde{b},$$

where $R \in \mathbb{C}$ and $\sigma(x)$ is a real-valued function which must be chosen properly and very carefully. The goal is to artificially damp the wave traveling inside the two layers to zero without modifying their dynamics in (a, b) by properly chosen R and $\sigma(x)$ [35,117,124,125]. Different choices have been proposed in the literatures [35,124,125]. Among them, the following choice works well for the NLSE/GPE (1.1) in 1D with cubic focusing nonlinearity [35,124,125]:

$$R = e^{i\pi/4}, \qquad \sigma(x) = \frac{1}{\delta^2}\begin{cases} (x-a)^2, & \tilde{a} \le x < a, \\ 0, & a \le x \le b, \\ (x-b)^2, & b < x \le \tilde{b}, \end{cases} \tag{2.27}$$

where δ is a positive constant. Then, the NLSE/GPE (1.1) with $d = 1$ will be truncated (or approximated) as

$$\begin{aligned} i\varepsilon\partial_t\psi(t,x) &= -\frac{\varepsilon^2}{2}\frac{1}{S(x)}\partial_x\left(\frac{1}{S(x)}\partial_x\psi(t,x)\right) \\ &\quad + V(x)\psi(t,x) + f(|\psi(t,x)|^2)\psi(t,x), \\ &\quad \tilde{a} < x < \tilde{b},\ t > 0, \end{aligned} \tag{2.28}$$

$$\psi(t,\tilde{a}) = \psi(t,\tilde{b}) = 0, \quad t \ge 0, \tag{2.29}$$

$$\psi(t=0,x) = \psi_0(x), \quad \tilde{a} \le x \le \tilde{b}. \tag{2.30}$$

The above problem can be discretized straightforwardly by CNFD, SIFD, ReFD and TSFD methods provided that we introduce the following finite difference operator to approximate $\frac{1}{S(x)}\partial_x\left(\frac{1}{S(x)}\partial_x d(x)\right)\Big|_{x=x_j}$ as

$$\begin{aligned} &\frac{1}{S(x)}\partial_x\left(\frac{1}{S(x)}\partial_x d(x)\right)\Big|_{x=x_j} \\ &\quad \approx \frac{1}{2h^2 S_j}\left[\frac{1}{S_{j-1/2}}d_{j-1} - \left(\frac{1}{S_{j-1/2}} + \frac{1}{S_{j+1/2}}\right)d_j + \frac{1}{S_{j+1/2}}d_{j+1}\right], \end{aligned}$$

where $S_j = S(x_j)$, $S_{j-1/2} = S(x_j - h/2)$ and d_j is the approximation of $d(x_j)$. This PML can be efficient and accurate for the NLSE/GPE in 1D in some cases if one can choose δ and R_0 properly. Of course, extensions to 2D and 3D are a little bit more difficult and it might give bad numerical results or even not work in some situations when one chooses improper layer function $S(x)$ and/or layer width R_0. Another way to design the PML is to introduce a damping potential which is also called as the complex absorbing potential (CAP) or exterior complex scaling (ECS) [135,136], i.e. choosing $S(x) \equiv 1$ for $\tilde{a} \le x \le \tilde{b}$ and replacing the real-valued potential $V(x)$ by a complex-valued potential $\tilde{V}(x) := V(x) - i\sigma(x)$, where $\sigma(x)$ is given in (2.27) with δ and R_0 two real positive constants to be determined based on the application. Then, the problem can be discretized by TSSP, CNFD, SIFD, ReFD and TSFD methods straightforwardly. Again, this CAP or ECS can be efficient and accurate for the NLSE/GPE in 1D in some situations if one can choose δ and R_0 suitably. The extensions to the 2D and 3D cases are direct. It might also lead to large inaccuracies in the calculations, more particularly for nonlinear problems. In general, PMLs are more robust from the accuracy point of view [128].

Another way is to find the Dirichlet-to-Neumann (DtN) map for the Schrödinger operator without and/or with external potential and nonlinearity at the boundary of the bounded computational domain by using the continuous and/or discrete Laplace transform [35,117,126,127,129–131,137,138]. The DtN map is usually nonlocal and a time-dependent pseudo-differential operator, and thus its approximations, which involve time fractional derivatives and integrals, are usually used in practical computations. These boundary conditions are also called as absorbing (or artificial or transparent) boundary conditions according to their properties. The goal is to avoid or at least to minimize the wave reflected back inside the domain while it should be outgoing. Since there are several very nice review papers on this part, we omit the details here for brevity and refer to [35] and references therein. Due to the nonlocal ABCs at the artificial boundary, one can usually solve the problem on the bounded computational domain by the second-order finite difference, such as the ReFD or SIFD method. It is usually very hard to design the spectral order method in space for the NLSE/GPE with nonlocal ABCs.

For the comparison of the performance and effectiveness of different PMLs and/or ABCs for the NLSE/GPE and their applications, we refer the reader to [129,139–142] and references therein.

2.4. Numerical methods in the semiclassical regime

When $0 < \varepsilon \ll 1$ in the NLSE/GPE (1.1), i.e. in the semiclassical limit regime, then the solution propagates waves with wave length at $\mathcal{O}(\varepsilon)$ in both space and time [20,37,38,47,143,144]. The highly oscillatory nature brings severe numerical burdens in numerical computation of the solution of the NLSE/GPE (1.1) [20,47,145]. In fact, in order to capture numerically "correct" physical observables such as density and current, different numerical methods request different mesh strategies (or ε-scalability) for discretizing the NLSE/GPE (1.1) in the semiclassical limit regime, i.e. $0 < \varepsilon \ll 1$. Based on the analysis and extensive numerical studies [20,37,38,47], it has been found that the ε-scalability for TSSP is mesh size $h = \mathcal{O}(\varepsilon)$, and time step $\tau = \mathcal{O}(1)$-independent of ε and $\tau = \mathcal{O}(\varepsilon)$ for the linear Schrödinger equation and NLSE/GPE, respectively; for the CNFD, ReFD, SIFD and TSFD as well as many other finite difference methods, the mesh size is $h = o(\varepsilon)$ and the time step is $\tau = o(\varepsilon)$ [37,38,47,48,146]. Thus, among those numerical methods for discretizing the NLSE/GPE (1.1) directly, the TSSP method has the best resolution in the semiclassical limit regime.

Of course, there are many other efficient and accurate numerical methods for solving the NLSE/GPE (1.1) based on the oscillatory structure of the solution. For the linear Schödinger equation, the Gaussian beam method [47,147–151] and the Gaussian wave packet transform method [152] show good resolution in spatial discretization, which in general requires $h = \mathcal{O}\left(\sqrt{\varepsilon}\right)$ and $\tau = \mathcal{O}(1)$-independent of ε. For the details of the Gaussian beam method, we refer the reader to a recent nice review paper [47] and references therein. However, in general, the Gaussian beam method cannot be extended to deal with the NLSE/GPE (1.1) due to the fact that the superposition is used in the method. We also mention here that there are some numerical methods in the literatures for solving the linear Schrödinger equation based on the Liouville equation through the Wigner transform, which can give good results in the linear case in the semiclassical limit regime [47,144,145].

Another approach for dealing with the nonlinear (or linear) Schrödinger equation (1.1) in the semiclassical limit regime is through the Madelung (or WKB) expansion [143,153]. In the semiclassical limit regime, i.e. $0 < \varepsilon \ll 1$, we denote the solution ψ to the NLSE/GPE (1.1) as ψ^ε and use the following WKB ansatz (or Madelung transformation) [47,143,153]:

$$\psi^\varepsilon(t,\mathbf{x}) = \sqrt{\rho^\varepsilon(t,\mathbf{x})}\ \exp\left(\frac{i S^\varepsilon(t,\mathbf{x})}{\varepsilon}\right), \quad \mathbf{x}\in\mathbb{R}^d,\ t\geq 0, \quad (2.31)$$

where the real-valued functions $\rho^\varepsilon = |\psi^\varepsilon|^2$ and S^ε are the density and phase, respectively. Plugging the above WKB ansatz into the NLSE/GPE (1.1) and identifying real and imaginary parts, the NLSE/GPE is reformulated as a coupled system for density and quantum velocity $v^\varepsilon = \nabla S^\varepsilon$, which is known as quantum hydrodynamic (QHD) system (made of a compressible, isentropic Euler system with Bohm potential) [143,154]. This model was used in [102,145,154–156] to build an asymptotic preserving (AP) scheme which allows us to compute numerical solution with time step and mesh size independent of ε. However, the QHD system fails to represent the solution of the original NLSE/GPE near vacuum, i.e. $\rho^\varepsilon = 0$ [143,154], and thus the scheme in [155] suffers from difficulties when the density ρ^ε vanishes in the domain and/or shocks or sharp changes happen in the QHD system. To overcome this drawback in the Madelung (or WKB) expansion for including vacuum, Grenier [157] introduced a modified Madelung (or WKB) expansion with the following ansatz [143,157]:

$$\psi^\varepsilon(t,\mathbf{x}) = A^\varepsilon(t,\mathbf{x})\ \exp\left(\frac{i S^\varepsilon(t,\mathbf{x})}{\varepsilon}\right), \quad \mathbf{x}\in\mathbb{R}^d,\ t\geq 0, \quad (2.32)$$

where $A^\varepsilon := a^\varepsilon + i\,b^\varepsilon$ is a complex-valued function with a^ε and b^ε two real-valued functions. Plugging (2.32) into the NLSE/GPE (1.1) and collecting $O(1)$ and $O(\varepsilon)$-terms, one obtains a system for A^ε and S^ε (or $v^\varepsilon = \nabla S^\varepsilon$) [143,157]. Based on this formulation, an AP scheme was proposed in [158], which works up to the time when caustics happens. More recently, another AP scheme [156,159] was presented based on Grenier's expansion with a regularized term, which can work after the caustics happens. For more details, we refer the reader to [158,159] and references therein.

3. Extension to the NLSE/GPE with damping and angular rotation terms

3.1. For the damped NLSE/GPE

As proven in [7,9,29], finite time blow-up may happen for the NLSE/GPE (1.1) with a focusing nonlinearity, e.g. the cubic nonlinearity (1.3) with $\beta < 0$ in 2D/3D. However, the physical quantities modeled by $\psi := \psi(t,\mathbf{x})$ do not become infinite, e.g. in BEC, which implies that the validity of (1.1) breaks down near the singularity. Additional physical mechanisms, which were initially small, become important near the singular point and prevent the formation of the singularity [32,33,160]. In BEC, the particle density $\rho := |\psi|^2$ becomes large close to the critical point and inelastic collisions between particles which are negligible for small densities become important [32,33,160,161]. Therefore, a small damping (absorption) term is introduced into the NLSE/GPE (1.1) which describes inelastic processes [9,32,33,160–162]. We are interested in the cases where these damping mechanisms are important and, therefore, restrict ourselves to the case of focusing nonlinearity, i.e. $\beta < 0$, where β may also be time dependent. We consider the following damped NLSE/GPE [9,32,33,161,162]:

$$\begin{aligned} i\,\partial_t\psi(t,\mathbf{x}) \;=\; & -\frac{1}{2}\nabla^2\psi(t,\mathbf{x}) + V(\mathbf{x})\,\psi(t,\mathbf{x}) \\ & + f(|\psi(t,\mathbf{x})|^2)\psi(t,\mathbf{x}) \\ & - i\,g(|\psi(t,\mathbf{x})|^2)\psi(t,\mathbf{x}), \quad t>0,\ \mathbf{x}\in\mathbb{R}^d, \end{aligned} \quad (3.1)$$

$$\psi(t=0,\mathbf{x}) = \psi_0(\mathbf{x}), \quad \mathbf{x}\in\mathbb{R}^d, \quad (3.2)$$

where $g(\rho)\geq 0$ for $\rho := |\psi|^2 \geq 0$ is a real-valued monotonically increasing function.

The general form of (3.1) covers many damped NLSEs/GPEs arising in various different applications. In BEC, for example, when $g(\rho) \equiv 0$, (3.1) reduces to the usual NLSE/GPE (1.1); a linear damping term $g(\rho)\equiv\delta$ with $\delta>0$ describes inelastic collisions with the background gas; cubic damping $g(\rho)=\delta_1\rho$ with $\delta_1>0$ corresponds to two-body loss [101]; and a quintic damping term of the form $g(\rho)=\delta_2\rho^2$ with $\delta_2>0$ adds three-body loss to the NLSE/GPE (1.1) [101]. It is easy to see that the decay of the *mass* according to (3.1) due to damping is given by

$$\begin{aligned} \dot N(t) &= \frac{d}{dt}\int_{\mathbb{R}^d} |\psi(t,\mathbf{x})|^2\,d\mathbf{x} \\ &= -2\int_{\mathbb{R}^d} g(|\psi(t,\mathbf{x})|^2)|\psi(t,\mathbf{x})|^2\,d\mathbf{x} \leq 0, \quad t>0. \end{aligned} \quad (3.3)$$

Particularly, if $g(\rho)\equiv\delta$ with $\delta>0$, the mass is given by

$$\begin{aligned} N(t) &= \int_{\mathbb{R}^d} |\psi(t,\mathbf{x})|^2\,d\mathbf{x} = e^{-2\delta t}N(0) \\ &= e^{-2\delta t}\int_{\mathbb{R}^d} |\psi_0(\mathbf{x})|^2\,d\mathbf{x}, \quad t\geq 0. \end{aligned} \quad (3.4)$$

Due to the appearance of the damping term, new ideas are needed to deal with them and different numerical methods have been presented in the literatures [161,162]. In fact, the numerical

methods such as TSSP, CNFD, ReFD, SIFD and TSFD methods for the NLSE/GPE (1.1) presented in the previous section can easily be extended to the damped NLSE/GPE (3.1). For simplicity of notations, here we only present the TSSP method for (3.1) with the quintic damping term in 1D, i.e. $d = 1$ and $g(\rho) = \delta_2\rho^2$ with $\delta_2 > 0$. From time $t = t_n$ to time $t = t_{n+1}$, the damped NLSE/GPE (3.1) is solved in two steps. One solves

$$i\,\partial_t\psi(t,x) = -\frac{1}{2}\partial_{xx}\psi(t,x), \quad a < x < b,\ t > t_n, \tag{3.5}$$

with the homogeneous Dirichlet boundary condition for one time step of length τ, followed by solving

$$\begin{aligned} i\,\partial_t\psi(t,x) &= V(x)\psi(t,x) + f(|\psi(t,x)|^2)\psi(t,x) \\ &\quad - i\,\delta_2|\psi(t,x)|^4\psi(t,x), \quad a \le x \le b,\ t > t_n, \end{aligned} \tag{3.6}$$

for the same time step τ. Again, Eq. (3.5) is discretized in space by the sine-spectral method and integrated in time *exactly*. For $t \in [t_n, t_{n+1}]$, multiplying the ODE (3.6) by $\overline{\psi(t,x)}$ and then subtracting from its conjugate, we obtain for $\rho(t,x) := |\psi(t,x)|^2$ [161]

$$\partial_t\,\rho(t,x) = -2\delta_2\,\rho^3(t,x), \quad t > t_n,\ a \le x \le b, \tag{3.7}$$

which can be solved analytically as

$$\rho(t,x) = \frac{\rho(t_n,x)}{\sqrt{4\delta_2(t-t_n) + \rho^2(t_n,x)}}, \quad t \ge t_n,\ a \le x \le b. \tag{3.8}$$

Plugging (3.8) into (3.6), we get a linear ODE as

$$\begin{aligned} i\,\partial_t\psi(t,x) &= \left[V(x) + f\left(\frac{\rho(t_n,x)}{\sqrt{4\delta_2(t-t_n)+\rho^2(t_n,x)}}\right)\right. \\ &\quad \left. - i\,\delta_2\frac{\rho^2(t_n,x)}{4\delta_2(t-t_n)+\rho^2(t_n,x)}\right]\psi(t,x), \\ &\quad t > t_n,\ a \le x \le b, \end{aligned} \tag{3.9}$$

which can be integrated *exactly* as for $0 \le s \le \tau$ and $a \le x \le b$

$$\begin{aligned} \psi(t_n+s,x) &= \psi(t_n,x)\ \exp\left[-i\left(V(x)s\right.\right. \\ &\quad + \frac{i}{4}\rho^2(t_n,x)\ln\frac{\rho^2(t_n,x)}{4\delta_2 s + \rho^2(t_n,x)} \\ &\quad \left.\left. + \int_0^s f\left(\frac{\rho(t_n,x)}{\sqrt{4\delta_2 u + \rho^2(t_n,x)}}\right)du\right)\right]. \end{aligned} \tag{3.10}$$

For cubic nonlinearity, the last term in the above equation can be integrated *analytically*. For a more general nonlinearity, if it cannot be integrated analytically, one can use a numerical quadrature, e.g. Simpson's rule, to evaluate it numerically [161,162]. Then, we can construct the second-order time-splitting sine pseudospectral (TSSP) method for the damped NLSE/GPE (3.1) *via* the Strang splitting [161,162]; the details are omitted here for brevity.

3.2. NLSE/GPE with an angular rotation term

In view of potential applications of BEC, the study of quantized vortices, which are related to superfluid properties, is one of the key issues. Currently, one of the most popular ways to generate quantized vortices from the BEC ground state is as follows: impose a laser beam rotating with an angular velocity on the magnetic trap holding the atoms to create a harmonic anisotropic potential. Various experiments have confirmed the observation of quantized vortices in BEC under a rotational frame [9,16,94,163–165]. At temperatures T much smaller than the critical temperature T_c, a BEC in a rotational frame is well described by the macroscopic wave function $\psi := \psi(t,\mathbf{x})$, whose evolution is governed by the following dimensionless GPE with an angular momentum rotation term around the z-axis [5,9,16,62,164,166,167]:

$$\begin{aligned} i\,\partial_t\psi(t,\mathbf{x}) &= -\frac{1}{2}\nabla^2\psi(t,\mathbf{x}) + V(\mathbf{x})\psi(t,\mathbf{x}) \\ &\quad + \beta|\psi(t,\mathbf{x})|^2\psi(t,\mathbf{x}) \\ &\quad - \Omega L_z\,\psi(t,\mathbf{x}), \quad \mathbf{x} \in \mathbb{R}^d,\ t > 0, \end{aligned} \tag{3.11}$$

with initial data

$$\psi(t=0,\mathbf{x}) = \psi_0(\mathbf{x}), \quad \mathbf{x} \in \mathbb{R}^d, \tag{3.12}$$

where $d = 2$ or 3 for 2D and 3D, respectively, β is a dimensionless constant describing the interaction strength, $V := V(\mathbf{x})$ is a given real-valued potential which is usually chosen as a harmonic potential, Ω is the dimensionless rotation velocity, and

$$L_z = -i\left(x\partial_y - y\partial_x\right) \tag{3.13}$$

is the z-component of the angular momentum operator $\boldsymbol{L} = (L_x, L_y, L_z)^T$ given by $\boldsymbol{L} = \mathbf{x} \wedge \boldsymbol{P}$, with the momentum $\boldsymbol{P} = -i\nabla$. The appearance of the angular momentum term means that we are using a reference frame where the trap is at rest. The above GPE is *time reversible* and *time transverse invariant* and it conserves the *mass* (1.4) and the *energy* defined as [5,9,16,62,164,166,167]

$$\begin{aligned} E(t) &:= \int_{\mathbb{R}^d}\left[\frac{1}{2}|\nabla\psi(t,\mathbf{x})|^2 + V(\mathbf{x})|\psi(t,\mathbf{x})|^2\right. \\ &\quad \left. + \frac{\beta}{2}|\psi(t,\mathbf{x})|^4 - \Omega\overline{\psi(t,\mathbf{x})}\,L_z\psi(t,\mathbf{x})\right]d\mathbf{x} \\ &\equiv E(0), \quad t \ge 0. \end{aligned} \tag{3.14}$$

Due to the appearance of the angular momentum term, new difficulties are introduced in solving the GPE (3.11) for rotating BEC numerically. Several efficient and accurate numerical methods have been proposed in the literatures for discretizing it [9,57,94,101,166,168–170]. In fact, the numerical methods such as TSSP, CNFD, ReFD, SIFD and TSFD methods for the NLSE/GPE (1.1) presented in the previous section can be easily extended to the GPE (3.11) with an angular momentum rotation. For conciseness, we present here only the TSSP method for (3.11) in 2D, i.e. $d = 2$.

From time $t = t_n$ to $t = t_{n+1}$, the GPE (3.11) is solved in two steps. One solves

$$i\,\partial_t\psi(t,\mathbf{x}) = -\frac{1}{2}\nabla\psi(t,\mathbf{x}) - \Omega L_z\,\psi(t,\mathbf{x}), \quad t > t_n, \tag{3.15}$$

for one time step of length τ, followed by solving the ODE

$$i\,\partial_t\psi(t,\mathbf{x}) = V(x)\psi(t,\mathbf{x}) + \beta|\psi(t,\mathbf{x})|^2\psi(t,\mathbf{x}), \quad t > t_n, \tag{3.16}$$

for the same time step τ. Similar to (2.17), Eq. (3.16) can be solved *analytically* [9,168]. Some numerical methods have been presented for discretizing (3.15). One numerical method is to adapt the polar coordinates (r,θ) in 2D such that the angular momentum rotation becomes the constant coefficient, and then to discretize it in the θ-direction by the Fourier spectral method, in the r-direction by the second-order or fourth-order finite difference method or finite element method, and in time by the Crank–Nicolson method. For more details, we refer the reader to [9,168]. Another method is to apply the Alternating Direction Implicit (ADI) method to decouple (3.15) into two sub-problems as

$$i\,\partial_t\psi(t,\mathbf{x}) = -\frac{1}{2}\partial_{xx}\psi(t,\mathbf{x}) - i\Omega y\partial_x\,\psi(t,\mathbf{x}), \quad t > t_n, \tag{3.17}$$

$$i\,\partial_t\psi(t,\mathbf{x}) = -\frac{1}{2}\partial_{yy}\psi(t,\mathbf{x}) + i\Omega x\partial_y\,\psi(t,\mathbf{x}), \quad t > t_n. \tag{3.18}$$

Now the first problem (3.17) is the constant coefficient with respect to x and the second problem (3.18) is the constant coefficient with respect to y, and thus they can be discretized in space by the Fourier spectral method and integrated in time *exactly*. Again, for more details, we refer the reader to [9,166].

A different way to apply the time-splitting technique to the GPE (3.11) is as follows: from time $t = t_n$ to time $t = t_{n+1}$, one solves

$$i\,\partial_t \psi(t,\mathbf{x}) = -\frac{1}{2}\nabla^2\psi(t,\mathbf{x}) + \frac{|\mathbf{x}|^2}{2}\psi(t,\mathbf{x}) - \Omega L_z\,\psi(t,\mathbf{x}), \quad \mathbf{x}\in\mathbb{R}^2,\ t > t_n, \tag{3.19}$$

for one time step of length τ, followed by solving

$$i\,\partial_t \psi(t,\mathbf{x}) = \left(V(x) - \frac{|\mathbf{x}|^2}{2}\right)\psi(t,\mathbf{x}) + \beta|\psi(t,\mathbf{x})|^2\psi(t,\mathbf{x}), \quad \mathbf{x}\in\mathbb{R}^2,\ t > t_n, \tag{3.20}$$

for the same time step τ. Again, similar to (2.17), Eq. (3.20) can be solved *analytically* [9,169]. Eq. (3.19) can be discretized in space by the generalized-Laguerre–Fourier spectral method and integrated in time *exactly*. One of the advantages of this method is that there is no need to truncate the original GPE (3.11) onto a bounded computational domain. Again, for more details, we refer the reader to [9,169].

Very recently, a simple and efficient numerical method has been proposed for discretizing the GPE (3.11) *via* a rotating Lagrangian coordinate [170–172]. For any time $t \geq 0$, let $A(t)$ be an orthogonal rotational matrix defined as

$$A(t) = \begin{pmatrix} \cos(\Omega t) & \sin(\Omega t) \\ -\sin(\Omega t) & \cos(\Omega t) \end{pmatrix}, \quad \text{if } d = 2, \tag{3.21}$$

and

$$A(t) = \begin{pmatrix} \cos(\Omega t) & \sin(\Omega t) & 0 \\ -\sin(\Omega t) & \cos(\Omega t) & 0 \\ 0 & 0 & 1 \end{pmatrix}, \quad \text{if } d = 3. \tag{3.22}$$

It is easy to verify that $A^{-1}(t) = A^T(t)$ for any $t \geq 0$ and $A(0) = I$, with I the identity matrix. For any $t \geq 0$, we introduce the *rotating Lagrangian coordinates* $\tilde{\mathbf{x}}$ as [171,172]

$$\tilde{\mathbf{x}} = A^{-1}(t)\mathbf{x} = A^T(t)\mathbf{x} \Leftrightarrow \mathbf{x} = A(t)\tilde{\mathbf{x}}, \quad \mathbf{x}\in\mathbb{R}^d \tag{3.23}$$

and denote the wave function in the new coordinates as $\phi := \phi(t,\tilde{\mathbf{x}})$

$$\phi(t,\tilde{\mathbf{x}}) := \psi(t,\mathbf{x}) = \psi\left(t, A(t)\tilde{\mathbf{x}}\right), \quad \mathbf{x}\in\mathbb{R}^d,\ t \geq 0. \tag{3.24}$$

In fact, here we refer the Cartesian coordinates $(t,\mathbf{x})$ to as the *Eulerian coordinates* and $(t,\tilde{\mathbf{x}})$ to as the rotating Lagrangian coordinates for any fixed $t \geq 0$. Using the chain rule, we obtain the following d-dimensional GPE in the rotating Lagrangian coordinates without the angular momentum rotation term [170,171]:

$$i\partial_t\phi(t,\tilde{\mathbf{x}}) = \left[-\frac{1}{2}\nabla^2 + W(\tilde{\mathbf{x}},t) + \beta|\phi|^2\right]\phi(t,\tilde{\mathbf{x}}), \quad \tilde{\mathbf{x}}\in\mathbb{R}^d,\ t > 0, \tag{3.25}$$

where $W(\tilde{\mathbf{x}},t) = V(A(t)\tilde{\mathbf{x}})$ for $\tilde{\mathbf{x}}\in\mathbb{R}^d$ and $t \geq 0$. The initial data (3.12) can be transformed as

$$\phi(t=0,\tilde{\mathbf{x}}) = \psi(t=0,\mathbf{x}) = \psi_0(\mathbf{x}) := \phi_0(\mathbf{x}) = \phi_0(\tilde{\mathbf{x}}), \quad \tilde{\mathbf{x}} = \mathbf{x}\in\mathbb{R}^d. \tag{3.26}$$

Then the GPE (3.25) with the initial data (3.26) can be directly solved by the TSSP presented in Section 2. After obtaining the numerical solution $\phi(t,\tilde{\mathbf{x}})$ on a bounded computational domain, if it is needed to recover the original wave function $\psi(t,\mathbf{x})$ over a set of fixed grid points in the Cartesian coordinates $\mathbf{x}$, one can use the standard Fourier/sine interpolation operators from the discrete numerical solution $\phi(t,\tilde{\mathbf{x}})$ to construct an interpolation continuous function over the bounded computational domain [173,174], which can be used to compute $\psi(t,\mathbf{x})$ over a set of fixed grid points in the Cartesian coordinates $\mathbf{x}$ for any fixed time $t \geq 0$. For more details, we refer the reader to [170].

4. Extension to the coupled NLSEs/GPEs

In many applications, e.g. multi-components BEC [5,9,175,176] and/or the interaction of laser beams [1,2,12,177], coupled NLSEs/GPEs have been used for modeling different problems. For simplicity of notations, here we only consider coupled NLSEs/GPEs with two equations and cubic nonlinearity for two-components BEC and/or interaction of two laser beams. Extensions to coupled NLSEs/GPEs with more than two equations are straightforward. Consider [5,9,16,19,175,178,179]

$$\begin{aligned} i\partial_t\psi_1(t,\mathbf{x}) &= \left[-\frac{1}{2}\nabla^2 + V_1(\mathbf{x}) + \beta_{11}|\psi_1|^2 + \beta_{12}|\psi_2|^2\right]\psi_1 + \lambda\psi_2, \quad \mathbf{x}\in\mathbb{R}^d,\ t > 0, \\ i\partial_t\psi_2(t,\mathbf{x}) &= \left[-\frac{1}{2}\nabla^2 + V_2(\mathbf{x}) + \beta_{21}|\psi_1|^2 + \beta_{22}|\psi_2|^2\right]\psi_2 + \lambda\psi_1, \quad \mathbf{x}\in\mathbb{R}^d,\ t > 0, \end{aligned} \tag{4.1}$$

with initial data

$$\psi_1(t=0,\mathbf{x}) = \psi_1^{(0)}(\mathbf{x}), \quad \psi_2(t=0,\mathbf{x}) = \psi_2^{(0)}(\mathbf{x}), \quad \mathbf{x}\in\mathbb{R}^d. \tag{4.2}$$

Here $(\psi_1,\psi_2) := (\psi_1(\mathbf{x},t),\psi_2(\mathbf{x},t))$ is the dimensionless complex-valued macroscopic wave function, $V_1(\mathbf{x})$ and $V_2(\mathbf{x})$ are two given dimensionless real-valued external potentials, $\beta_{11}, \beta_{12} = \beta_{21}$ and β_{22} are given dimensionless real constants describing the interaction strength, and λ is a given dimensionless real constant describing internal atomic Josephson junction in a two-components BEC [5,9,19,175,179–181]. These coupled NLSEs/GPEs conserve the *total mass* as [5,9,19,175,179]

$$\begin{aligned} N(t) &= \int_{\mathbb{R}^d}\left(|\psi_1(t,\mathbf{x})|^2 + |\psi_2(t,\mathbf{x})|^2\right)d\mathbf{x} \\ &\equiv \int_{\mathbb{R}^d}\left(|\psi_1^{(0)}(\mathbf{x})|^2 + |\psi_2^{(0)}(\mathbf{x})|^2\right)d\mathbf{x} := N(0), \quad t \geq 0, \end{aligned} \tag{4.3}$$

and the *energy* as

$$\begin{aligned} E(t) &:= \int_{\mathbb{R}^d}\left[\frac{1}{2}\left(|\nabla\psi_1|^2 + |\nabla\psi_2|^2\right) + V_1(\mathbf{x})|\psi_1|^2 + V_2(\mathbf{x})|\psi_2|^2 + \frac{1}{2}\beta_{11}|\psi_1|^4 \right. \\ &\quad \left. + \frac{1}{2}\beta_{22}|\psi_2|^4 + \beta_{12}|\psi_1|^2|\psi_2|^2 + 2\lambda\cdot\mathrm{Re}(\psi_1\bar{\psi}_2)\right]d\mathbf{x} \\ &\equiv E(0), \quad t \geq 0, \end{aligned} \tag{4.4}$$

where $\mathrm{Re}(f)$ denotes the real part of the function f. In addition, if there is no internal Josephson junction in (4.1), i.e. $\lambda = 0$, the mass of each component is also conserved [5,9,19,175,179]

$$N_1(t) := \int_{\mathbb{R}^d}|\psi_1(t,\mathbf{x})|^2\,d\mathbf{x} \equiv \int_{\mathbb{R}^d}|\psi_1^{(0)}(\mathbf{x})|^2\,d\mathbf{x}, \quad N_2(t) := \int_{\mathbb{R}^d}|\psi_2(t,\mathbf{x})|^2\,d\mathbf{x} \equiv \int_{\mathbb{R}^d}|\psi_2^{(0)}(\mathbf{x})|^2\,d\mathbf{x}, \quad t \geq 0. \tag{4.5}$$

Table 2
Spatial error analysis on errors $e_\infty^{p,m}(t = 5)$ of different numerical methods for the NLSE/GPE (1.1) in 1D under different mesh sizes h.

h		$h_0 = 0.5$	$h_0/2$	$h_0/4$	$h_0/8$	$h_0/16$
CNFD	e_∞^p	2.48	1.87E0	4.28E−1	1.03E−1	2.57E−2
	e_∞^m	1.89	6.98E−1	1.46E−1	3.52E−2	8.68E−3
ReFD	e_∞^p	2.48	1.87E0	4.28E−1	1.03E−1	2.57E−2
	e_∞^m	1.89	6.98E−1	1.46E−1	3.52E−2	8.68E−3
SIFD	e_∞^p	2.48	1.87E0	4.28E−1	1.03E−1	2.57E−2
	e_∞^m	1.89	6.98E−1	1.46E−1	3.52E−2	8.68E−3
TSFD	e_∞^p	2.48	1.87E0	4.28E−1	1.03E−1	2.57E−2
	e_∞^m	1.89	6.98E−1	1.46E−1	3.52E−2	8.68E−3
TSSP	e_∞^p	1.485	3.81E−4	8.63E−9	<1E−9	<1E−9
	e_∞^m	1.408	2.45E−4	4.49E−9	<1E−9	<1E−9

Table 3
Temporal error analysis on errors $e_\infty^{p,m}(t = 5)$ of different numerical methods for the NLSE/GPE (1.1) in 1D under different time steps τ.

τ		$\tau_0 = 0.1$	$\tau_0/2$	$\tau_0/4$	$\tau_0/8$	$\tau_0/16$
CNFD	e_∞^p	2.62E−1	6.65E−2	1.64E−2	3.88E−3	7.28E−4
	e_∞^m	1.08E−2	2.87E−3	6.70E−4	1.16E−4	6.64E−5
ReFD	e_∞^p	3.11E−1	2.68E−2	1.97E−2	5.07E−3	1.47E−3
	e_∞^m	2.25E−1	5.37E−2	1.34E−2	3.37E−3	9.25E−4
SIFD	e_∞^p	2.96E0	6.46E−1	1.91E−1	6.62E−2	2.61E−2
	e_∞^m	2.57E−1	1.13E−1	5.34E−2	2.58E−2	1.26E−2
TSFD	e_∞^p	8.51E−1	2.00E−1	4.97E−2	1.25E−2	3.37E−3
	e_∞^m	4.10E−1	9.03E−2	2.20E−2	5.49E−3	1.44E−3
TSSP	e_∞^p	5.17E−1	1.40E−1	3.57E−2	8.98E−3	2.25E−3
	e_∞^m	4.98E−2	1.64E−2	4.21E−3	1.06E−3	2.65E−4

Different efficient and accurate numerical methods have been proposed in the literatures for discretizing the above coupled NLSEs/GPEs [9,19,175,179–181]. In fact, the extension of the numerical methods TSSP, CNFD, ReFD, SIFD and TSFD for the NLSE/GPE (1.1) presented in Section 2 is direct for the coupled NLSEs/GPEs (4.1). For simplicity of notations, here we present only the TSSP method for (4.1).

From time $t = t_n$ to time $t = t_{n+1}$, the coupled NLSEs/GPEs (4.1) are solved in two steps. One solves

$$\begin{aligned} i\partial_t \psi_1(t,\mathbf{x}) &= -\frac{1}{2}\nabla^2\psi_1(t,\mathbf{x}) + \lambda\psi_2(t,\mathbf{x}), \quad t > t_n, \\ i\partial_t \psi_2(t,\mathbf{x}) &= -\frac{1}{2}\nabla^2\psi_2(t,\mathbf{x}) + \lambda\psi_1(t,\mathbf{x}), \quad t > t_n, \end{aligned} \tag{4.6}$$

for one time step of length τ, followed by solving

$$\begin{aligned} i\partial_t \psi_1(t,\mathbf{x}) &= [V_1(\mathbf{x}) + \beta_{11}|\psi_1(t,\mathbf{x})|^2 \\ &\quad + \beta_{12}|\psi_2(t,\mathbf{x})|^2]\psi_1(t,\mathbf{x}), \quad t > t_n, \\ i\partial_t \psi_2(t,\mathbf{x}) &= [V_2(\mathbf{x}) + \beta_{21}|\psi_1(t,\mathbf{x})|^2 \\ &\quad + \beta_{22}|\psi_2(t,\mathbf{x})|^2]\psi_2(t,\mathbf{x}), \quad t > t_n, \end{aligned} \tag{4.7}$$

for the same time step τ. Similar to (2.16), Eq. (4.6) can be discretized in space by the sine spectral method and then integrated in time *exactly* [9,175,176,179]. Like for (2.17), for $t \in [t_n, t_{n+1}]$, Eq. (4.7) leaves $\rho_1 := |\psi_1|^2$ and $\rho_2 := |\psi_2|^2$ invariant [9,175,179], i.e. $\rho_1(t,\mathbf{x}) \equiv \rho_1(t_n,\mathbf{x})$ and $\rho_2(t,\mathbf{x}) \equiv \rho_2(t_n,\mathbf{x})$ for $t_n \le t \le t_{n+1}$ for any fixed $\mathbf{x}$; thus (4.7) can be integrated in time *exactly* [9,175,176,179]. Then, we can construct the second-order TSSP method for the coupled NLSEs/GPEs (4.1) *via* the Strang splitting [9,19,175,179,182]. We omit the details here for brevity.

We remark here that the above TSSP, CNFD, SIFD methods have been extended to solve many other nonlinear dispersive partial differential equations arising from different applications. For details, we refer the reader to the Schrödinger equation with wave operator [52,183], the Schödinger–Poisson system [24,37,184], the Zakharov system [54,55,185–187], the Klein–Gordon–Schrödinger equations [188], and the Ginzburg–Landau–Schrödinger equations [189] and references therein.

5. Numerical comparison and applications

5.1. Comparison of different numerical methods

In order to compare the numerical performance and accuracy of different numerical methods, such as TSSP, CNFD, SIFD, ReFD and TSFD, for the NLSE/GPE (1.1), we take $d = 1$, $\varepsilon = 1$, $V(x) \equiv 0$ and $f(\rho) = -\rho$ in (1.1), and the initial data ψ_0 in (1.2) as

$$\psi_0(x) = A\ \mathrm{sech}(A(x - x_0))\, e^{i(vx+\theta_0)}, \quad x \in \mathbb{R},$$

with $A = 2$, $v = 1$ and $x_0 = \theta_0 = 0$. Then the NLSE/GPE (1.1) with (1.2) has the exact bright soliton solution (1.8), i.e. $\psi(t,x) = \psi_B(t,x)$, with $\beta = -1$, $A = 2$, $v = 1$ and $x_0 = \theta_0 = 0$. In our computation, we take the bounded computational domain as the interval (a, b) with $a = -15$ and $b = 20$ and the homogeneous Dirichlet boundary condition, which are large enough so that the truncation errors can be ignored. In order to quantify the numerical solution, we use the l^∞-norm of the error between the numerical solution ψ_j^n and the exact solution $\psi(t_n, x_j)$ as

$$\begin{aligned} e_\infty^p(t_n) &:= \max_{0\le j\le J} |\psi(t_n, x_j) - \psi_j^n|, \\ e_\infty^m(t_n) &:= \max_{0\le j\le J} (|\psi(t_n, x_j)| - |\psi_j^n|), \quad n \ge 0. \end{aligned} \tag{5.1}$$

The functions e_∞^p and e_∞^m allow us respectively to measure the phase error and the modulus error.

To test the spatial discretization errors of the different numerical methods, we fix $\tau = 10^{-5}$ such that the time discretization errors are negligible. Table 2 shows the spatial errors $e_\infty^{p,m}(t = 5)$

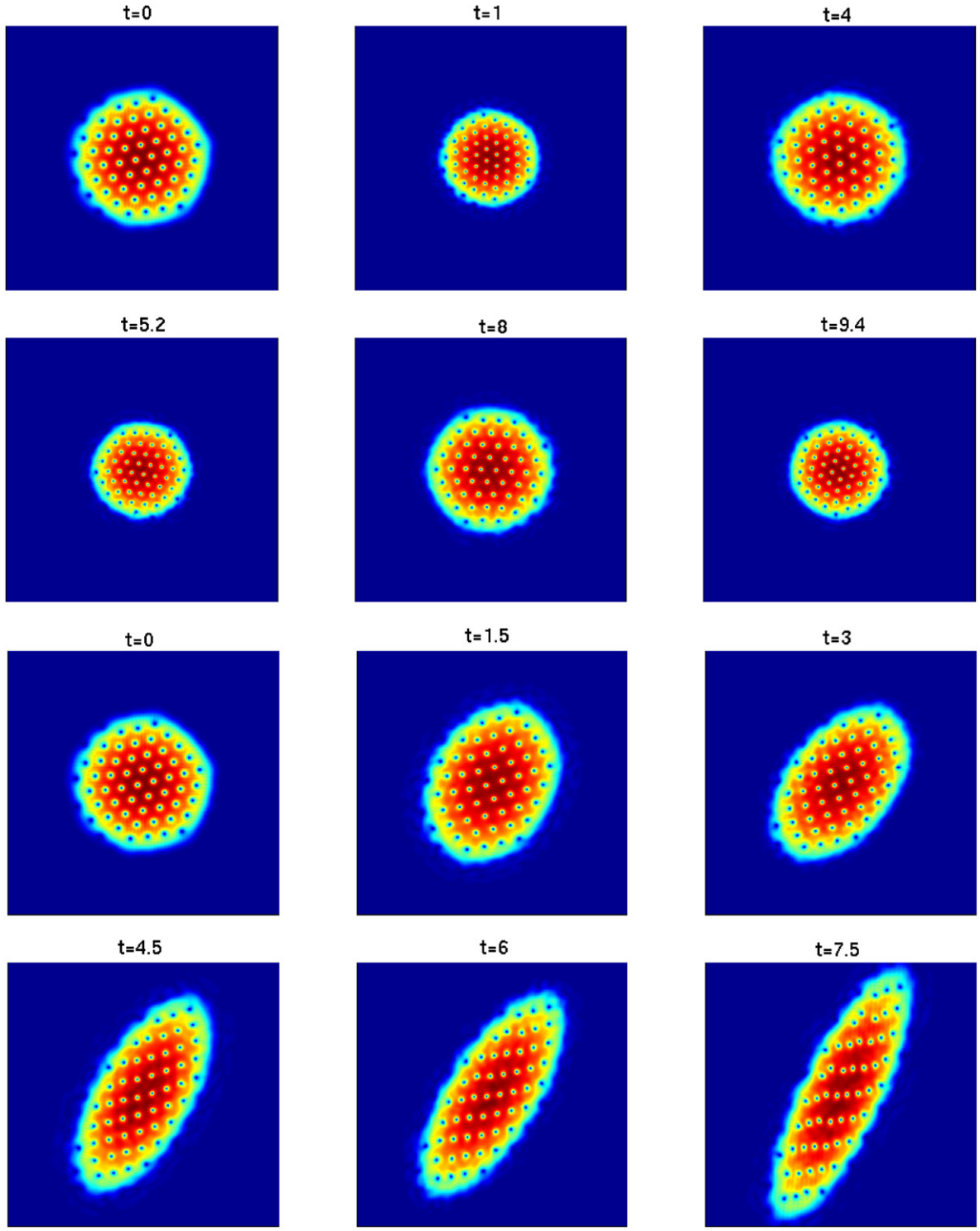

Fig. 1. Contour plots of the density function $\rho := |\psi(t, \mathbf{x})|^2$ for the dynamics of a quantized vortex lattice in a rotating BEC for case I (top two rows) and case II (bottom two rows).

for different numerical methods under different mesh sizes h. Similarly, to compare the temporal discretization errors of different numerical methods, we take $h = 3.5 \times 10^{-3}$ to get very small spatial discretization errors. Table 3 shows the temporal errors $e_\infty^{p,m}(t = 5)$ for different numerical methods under different time steps τ [31].

From Tables 2 and 3 as well as additional numerical results not shown here for brevity, it is clearly demonstrated that TSSP is spectral order accurate in space and second-order accurate in time while CNFD, ReFD, SIFD and TSFD are second-order accurate in both space and time. For more numerical comparisons, we refer the reader to [9,31,53] and references therein.

5.2. Applications

In order to show numerical results for problems coming from applications, we consider the dynamics of the NLSE/GPE (3.11) with a rotation term in 2D starting from a quantized vortex lattice

for a rotating BEC [9,57,166,169,170], i.e. we take $d = 2$, $\beta = 1000$ and $\Omega = 0.9$ in (3.11). The initial datum in (3.12) is chosen as a stationary vortex lattice which is computed numerically by using the method in [9,190] with the above parameters and the harmonic potential $V(x, y) = \frac{1}{2}(x^2 + y^2)$. Then, the dynamics of the vortex lattice is studied numerically by perturbing the harmonic potential from $V(x, y) = \frac{1}{2}(x^2 + y^2)$ to $V(x, y) = \frac{1}{2}(\gamma_x^2 x^2 + \gamma_y^2 y^2)$ with (i) case I: $\gamma_x = \gamma_y = 2$, and (ii) case II: $\gamma_x = 1.1$ and $\gamma_y = 0.9$, respectively, at time $t = 0$. In the numerical simulation, we choose the bounded computational domain as $[-32, 32]^2$ with the homogeneous Dirichlet boundary condition, mesh size $h = 1/16$ and time step $\tau = 10^{-4}$. Fig. 1 shows the contour plots of the density function $\rho(t, \mathbf{x}) := |\psi(t, \mathbf{x})|^2$ displayed on $[-17, 17]^2$ at different times for cases I and II.

6. Conclusion and perspectives

Due to its massive applications in many different areas, the research on numerical methods and simulation as well as applications related to the nonlinear Schrödinger/Gross–Pitaevskii equations (NLSE/GPE) has been started several decades ago. Up to now, rich and extensive research results have been obtained in developing and analyzing efficient and accurate numerical methods for the NLSE/GPE and in applying them for simulating problems arising from many different areas, such as Bose–Einstein condensation (BEC), nonlinear optics, superfluids, etc. Nowadays, numerical simulation has become a very important tool in theoretical and computational physics as well as computational and applied mathematics for solving problems related to the NLSE/GPE and it has been used to predict and guide new experiments due to the advances in numerical methods and their analysis as well as powerful and/or parallel computers. Of course, due to its dispersive nature of the NLSE/GPE, when one is doing numerical simulation, he/she should choose the numerical method, mesh size and time step as well as the computational domain properly and carefully so that the numerical results reflect "correct" physical phenomena.

The research in this area is still very active and highly demanded due to the latest experimental and/or technological advances in BEC, nonlinear optics, graphene, semiconductors, topological insulators, materials simulation and design, etc. It becomes more and more interdisciplinary involving theoretical, computational and experimental physicists and computational and applied mathematicians as well as computational scientists. Of course, there are still many important issues to be addressed. For example, extension and designing as well as analyzing new numerical methods for highly oscillatory nonlinear dispersive partial differential equations, especially coupled NLSE/GPE with other equations such as the Davey–Stewartson system [7], Kadomtsev–Petviashvili equations [7], coupled NLSE/GPE with quantum Boltzmann equation for BEC at finite temperature [9,191], etc., are always welcome and highly demanded. Another issue is to design efficient and accurate numerical methods and apply them for studying numerically NLSE/GPE with random potential [22,80–82] or stochastic NLSE/GPE [192–196] with applications and NLSE/GPE in higher dimensions, i.e. $d > 3$ for many-body problems in quantum chemistry and materials simulation and design. Here memory and computational cost might be extremely high and thus parallel computing and/or sparse grids as well as spatial and temporal adaptivities are very useful and essential. Last but not the least, efficient implementation of numerical methods and portable and readable programming are very important from the application point of view. Although there are plenty of research codes available in the community [90,197–199], a software package or tool box (with parallel implementation in 2D and 3D) is still very useful for applications. In summary, in order to solve challenging scientific and engineering problems and/or guiding and predicting new experiments related to NLSE/GPE, the interaction and close collaboration between computational and applied mathematicians and theoretical and experimental physicists and chemists as well as computational and applied scientists become more and more essential in this research area.

Acknowledgments

This work was partially supported by the French ANR grants MicroWave NT09_460489 ("Programme Blanc" call) and ANR-12-MONU-0007-02 BECASIM ("Modèles Numériques" call) (X. Antoine and C. Besse), and by the Singapore A*STAR SERC "Complex Systems" Research Programme grant 1224504056 (W. Bao).

References

[1] F. Abdullaev, S. Darmanyan, P. Khabibullaev, Optical Solitons, Springer-Verlag, New York, 1993.
[2] M.J. Ablowitz, H. Segur, Solitons and the Inverse Scattering Transform, SIAM, Philadelphia, 1981.
[3] T. Dauxois, M. Peyrard, Physics of Solitons, Cambridge University Press, 2006.
[4] P.A.M. Dirac, The Principles of Quantum Mechanics, Oxford University Press, 1958.
[5] L.P. Pitaevskii, S. Stringari, Bose–Einstein Condensation, Clarendon Press, Oxford, 2003.
[6] E. Schrödinger, Phys. Rev. 28 (1926) 1049.
[7] C. Sulem, P. Sulem, The Nonlinear Schrödinger Equation: Self-Focusing and Wave Collapse, Springer, 1999.
[8] M.H. Anderson, J.R. Ensher, M.R. Matthewa, C.E. Wieman, E.A. Cornell, Science 269 (1995) 198.
[9] W. Bao, Y. Cai, Kinet. Relat. Models 6 (2013) 1.
[10] E.P. Gross, Nuovo Cimento 20 (1961) 454.
[11] L.P. Pitaevskii, Zh. Eksp. Teor. Fys. 40 (1961) 646. [Sov. Phys. JETP 13 (1961) 451].
[12] A.C. Newell, Solitons in Mathematics and Physics, SIAM, Philadelphia, 1985.
[13] P.A. Markowich, Applied Partial Differential Equations: A Visual Approach, Springer, 2007.
[14] P.A. Markowich, C.A. Ringhofer, C. Schmeiser, Semiconductor Equations, Springer-Verlag, 2002.
[15] E.D. Engel, M. Reiner, Density Functional Theory: An Advanced Course, Springer, 2011.
[16] A. Aftalion, Vortices in Bose–Einstein Condensates, Birkhäuser, Boston, 2006.
[17] C.F. Barenghi, R.J. Donnelly, W.F. Vinen, Quantized Vortex Dynamics and Superfluid Turbulence, Springer, 2001.
[18] A.S. Davydov, Solitons in Molecular Systems, Springer, 1991.
[19] W. Bao, Dynamics in Models of Coarsening, Coagulation, Condensation and Quantization, in: IMS Lecture Notes Series, vol. 9, World Scientific, 2007, p. 141.
[20] Z. Huang, S. Jin, P.A. Markowich, C. Sparber, SIAM J. Sci. Comput. 29 (2007) 515.
[21] Z. Huang, S. Jin, P.A. Markowich, C. Sparber, Multiscale Model. Simul. 7 (2008) 539.
[22] B. Min, T. Li, M. Rosenkranz, W. Bao, Phys. Rev. A 86 (2012) 053612.
[23] W. Bao, Y. Cai, H. Wang, J. Comput. Phys. 229 (2010) 7874.
[24] W. Bao, N.J. Mauser, H.P. Stimming, Commun. Math. Sci. 1 (2003) 809.
[25] C. Bardos, L. Erdős, F. Golse, N.J. Mauser, H.-T. Yau, C. R. Math. Acad. Sci. Paris 334 (2002) 515.
[26] Y. Cai, M. Rosenkranz, Z. Lei, W. Bao, Phys. Rev. A 82 (2010) 043623.
[27] B. Xiong, J. Gong, H. Pu, W. Bao, B. Li, Phys. Rev. A 79 (2009) 013626.
[28] W. Bao, H. Jian, N.J. Mauser, Y. Zhang, Dimension reduction of the Schrödinger equation with Coulomb and anisotropic confining potentials, Preprint.
[29] T. Cazenave, Semilinear Schrödinger Equations, in: Courant Lect. Notes Math., vol. 10, Amer. Math. Soc., Providence, R.I, 2003.
[30] L.I. Ignat, E. Zuazua, SIAM J. Numer. Anal. 47 (2009) 1366.
[31] W. Bao, Q. Tang, Z. Xu, J. Comput. Phys. 235 (2013) 423.
[32] G. Fibich, SIAM J. Appl. Math. 61 (2001) 1680.
[33] G. Fibich, G. Papanicolaou, SIAM J. Appl. Math. 60 (2000) 183.
[34] G.D. Akrivis, V.A. Dougalis, O.A. Karakashian, Numer. Math. 59 (1991) 31.
[35] X. Antoine, A. Arnold, C. Besse, M. Ehrhardt, A. Schädle, Commun. Comput. Phys. 4 (2008) 729.
[36] W. Bao, D. Jaksch, P.A. Markowich, J. Comput. Phys. 187 (2003) 318.
[37] W. Bao, S. Jin, P.A. Markowich, J. Comput. Phys. 175 (2002) 487.
[38] W. Bao, S. Jin, P.A. Markowich, SIAM J. Sci. Comput. 25 (2003) 27.
[39] C. Besse, SIAM J. Numer. Anal. 42 (2004) 934.
[40] T.F. Chan, D. Lee, L. Shen, SIAM J. Numer. Anal. 23 (1986) 274.
[41] T.F. Chan, L. Shen, SIAM J. Numer. Anal. 24 (1987) 336.
[42] M.M. Cerimele, M.L. Chiofalo, F. Pistella, S. Succi, M.P. Tosi, Phys. Rev. E 62 (2000) 1382.
[43] M.M. Cerimele, F. Pistella, S. Succi, Comput. Phys. Comm. 129 (2000) 82.
[44] A. Durán, J.M. Sanz-Serna, IMA J. Numer. Anal. 20 (2000) 235.
[45] B. Guo, J. Comput. Math. 4 (1986) 121.
[46] R.H. Hardin, F.D. Tappert, SIAM Rev. 15 (1973) 423.
[47] S. Jin, P.A. Markowich, C. Sparber, Acta Numer. (2011) 121.
[48] P.A. Markowich, P. Pietra, C. Pohl, Numer. Math. 81 (1999) 595.

[49] D. Pathria, J.L. Morris, J. Comput. Phys. 87 (1990) 108.
[50] T.R. Taha, M.J. Ablowitz, J. Comput. Phys. 55 (1984) 203.
[51] J.A.C. Weideman, B.M. Herbst, SIAM J. Numer. Anal. 23 (1986) 485.
[52] W. Bao, Y. Cai, SIAM J Numer. Anal. 50 (2012) 492.
[53] Q. Chang, E. Jia, W. Sun, J. Comput. Phys. 148 (1999) 397.
[54] Q. Chang, B. Guo, H. Jiang, Math. Comp. 64 (1995) 537.
[55] R.T. Glassey, Math. Comp. 58 (1992) 83.
[56] Y. Zhu, J. Comput. Math. 1 (1983) 116.
[57] W. Bao, Y. Cai, Math. Comp. 82 (2013) 99.
[58] G.D. Akrivis, IMA J. Numer. Anal. 13 (1993) 115.
[59] G.D. Akrivis, V.A. Dougalis, RAIRO Modél. Math. Anal. Numér. 25 (1991) 643.
[60] Q. Chang, G. Wang, J. Comput. Phys. 88 (1990) 362.
[61] T. Wang, J. Comput. Appl. Math. 25 (2011) 4237.
[62] W. Bao, J. Shen, SIAM J. Sci. Comput. 26 (2005) 2020.
[63] M. Caliari, Ch. Neuhauser, M. Thalhammer, J. Comput. Phys. 228 (2009) 822.
[64] M. Thalhammer, SIAM J. Numer. Anal. 46 (2008) 2022.
[65] W. Bao, Y. Zhang, Math. Models Methods Appl. Sci. 15 (2005) 1863.
[66] G. Strang, SIAM J. Numer. Anal. 5 (1968) 505.
[67] C. Besse, B. Bidégaray, S. Descombes, SIAM J. Numer. Anal. 40 (2002) 26.
[68] L. Gauckler, Ch. Lubich, Found. Comput. Math. 10 (2010) 275.
[69] Ch. Lubich, Math. Comp. 77 (2008) 2141.
[70] C. Neuhauser, M. Thalhammer, BIT 49 (2009) 199.
[71] J. Shen, Z.-Q. Wang, Found. Comput. Math. 13 (2013) 99.
[72] M. Thalhammer, SIAM J. Numer. Anal. 50 (2012) 3231.
[73] A. Debussche, E. Faou, SIAM J. Numer. Anal. 47 (2009) 3705.
[74] G. Dujardin, E. Faou, C. R. Math. Acad. Sci. Paris 344 (2007) 89.
[75] G. Dujardin, E. Faou, Numer. Math. 108 (2007) 223.
[76] E. Faou, Geometric Numerical Integration and Schrödinger Equations, European Mathematical Society, 2012.
[77] E. Faou, B. Grébert, Found. Comput. Math. 11 (2011) 381.
[78] S.A. Chin, C.R. Chen, J. Chem. Phys. 114 (2001) 7338.
[79] S.A. Chin, C.R. Chen, J. Chem. Phys. 117 (2002) 1409.
[80] P.W. Anderson, Phys. Rev. Lett. 109 (1958) 1492.
[81] Y. Dubi, Y. Meir, Y. Avishai, Nature 449 (2007) 876.
[82] J.E. Lye, L. Fallani, M. Modugno, D.S. Wiersma, C. Fort, M. Inguscio, Phys. Rev. Lett. 95 (2005) 070401.
[83] W. Bao, Q. Tang, Numerical study of quantized vortex interaction in nonlinear Schrödinger equation on bounded domain, Preprint.
[84] H. Wang, Appl. Math. Comput. 170 (2005) 17.
[85] M. Thalhammer, J. Abhau, J. Comput. Phys. 231 (2012) 6665.
[86] W. Bao, Methods Appl. Anal. 11 (2004) 367.
[87] M. Robinson, G. Fairweather, B. Herbst, J. Comput. Phys. 104 (1993) 227.
[88] J.M. Sanz-Serna, Math. Comp. 43 (1984) 21.
[89] J.M. Sanz-Serna, J.G. Verwer, IMA J. Numer. Anal. 6 (1986) 25.
[90] P. Muruganandam, S.K. Adhikari, Comput. Phys. Comm. 180 (2009) 1888.
[91] Y. Zhang, W. Bao, Appl. Numer. Math. 57 (2007) 697.
[92] S.K. Adhikari, Phys. Rev. E 62 (2000) 2937.
[93] R. Baer, Phys. Rev. A 62 (2000) 063810.
[94] B.M. Caradoc-Davis, R.J. Ballagh, K. Burnett, Phys. Rev. Lett. 83 (1999) 895.
[95] B.M. Caradoc-Davis, R.J. Ballagh, P.B. Blakie, Phys. Rev. A 62 (2000) 011602.
[96] H. Liao, Z. Sun, SIAM J. Numer. Anal. 47 (2010) 4381.
[97] S. Xie, G. Li, S. Yi, Comput. Methods Appl. Mech. Engrg. 198 (2009) 1052.
[98] M. Edwards, K. Burnett, Phys. Rev. A 51 (1995) 101103.
[99] Z. Gao, S. Xie, Appl. Numer. Math. 61 (2011) 595.
[100] P.A. Ruprecht, M.J. Holland, K. Burnett, M. Edwards, Phys. Rev. A 51 (1995) 4704.
[101] H. Saito, M. Ueda, Phys. Rev. Lett. 86 (2001) 1406.
[102] A. Arnold, N. Ben Abdallah, C. Negulescu, SIAM J. Numer. Anal. 49 (2011) 1436.
[103] Q. Chang, L. Xu, J. Comput. Math. 4 (1986) 191.
[104] M. Delfour, M. Fortin, G. Payre, J. Comput. Phys. 44 (1981) 277.
[105] C.M. Dion, E. Cances, Phys. Rev. E 67 (2003) 046706.
[106] W. Dörfler, Numer. Math. 73 (1998) 419.
[107] Z. Fei, V.M. Pérez-García, L. Vázquez, Appl. Math. Comput. 71 (1995) 165.
[108] D.F. Griffiths, A.R. Mitchell, J.L. Morris, Comput. Methods Appl. Mech. Engrg. 45 (1984) 177.
[109] J. Hong, L. Kong, Commun. Comput. Phys. 7 (2010) 613.
[110] J. Hong, X.-Y. Liu, C. Li, J. Comput. Phys. 226 (2007) 1968.
[111] J. Hong, Y. Liu, H. Munthe-Kaas, A. Zanna, Appl. Numer. Math. 56 (2006) 814.
[112] M.S. Ismail, T.R. Taha, Math. Comput. Simul. 56 (2001) 547.
[113] M.S. Ismail, T.R. Taha, Math. Comput. Simul. 74 (2007) 302.
[114] I. Kyza, C. Makridakis, M. Plexousakis, IMA J. Numer. Anal. 31 (2011) 416.
[115] L. Wu, SIAM J. Numer. Anal. 33 (1996) 1526.
[116] A. Gammal, T. Frederico, L. Tomio, Phys. Rev. E 60 (1999) 2421.
[117] A. Arnold, VLSI Des. 6 (1998) 313.
[118] A. Arnold, M. Ehrhardt, M. Schulte, I. Sofronov, Commun. Math. Sci. 10 (2012) 889.
[119] J.P. Bérenger, J. Comput. Phys. 114 (1994) 185.
[120] A. Bayliss, E. Turkel, Comm. Pure Appl. Math. 33 (1980) 707.
[121] B. Engquist, A. Majda, Math. Comp. 31 (1977) 629.
[122] G. Mur, IEEE Trans. Electromagn. Compat. 23 (1981) 377.
[123] G. Pang, L. Bian, S. Tang, Phys. Rev. E 86 (2012) 066709.
[124] A. Nissen, G. Kreiss, Commun. Comput. Phys. 9 (2011) 147.
[125] C. Zheng, J. Comput. Phys. 227 (2007) 537.
[126] X. Antoine, C. Besse, S. Descombes, SIAM J. Numer. Anal. 43 (2006) 2272.
[127] X. Antoine, C. Besse, P. Klein, J. Comput. Phys. 228 (2009) 312.
[128] X. Antoine, C. Besse, P. Klein, Laser Phys. 21 (2011) 1191.
[129] X. Antoine, C. Besse, P. Klein, SIAM J. Sci. Comput. 33 (2011) 1008.
[130] X. Antoine, C. Besse, P. Klein, Math. Models Methods Appl. Sci. 22 (2012) 50026.
[131] X. Antoine, C. Besse, P. Klein, Numer. Math. (2013) http://dx.doi.org/10.1007/s00211-013-0542-8.
[132] J. Szeftel, Numer. Math. 104 (2006) 103.
[133] J. Szeftel, SIAM J. Numer. Anal. 42 (2004) 1527.
[134] C. Zheng, J. Comput. Phys. 215 (2006) 552.
[135] A. Jüngel, J.F. Mennemann, Math. Comput. Simulation 81 (2010) 883.
[136] A. Scrinzi, Phys. Rev. A 81 (2010) 053845.
[137] J.S. Papadakis, M.I. Taroudakis, P.J. Papadakis, B. Mayfield, J. Acoust. Soc. Am. 92 (1992) 2030.
[138] X. Antoine, C. Besse, J. Comput. Phys. 188 (2003) 157.
[139] P. Klein, X. Antoine, C. Besse, M. Ehrhardt, Commun. Comput. Phys. 10 (2011) 1280.
[140] Z. Xu, H. Han, Phys. Rev. E 74 (2006) 037704.
[141] Z. Xu, H. Han, X. Wu, J. Comput. Phys. 225 (2007) 1577.
[142] J. Zhang, Z. Xu, X. Wu, Phys. Rev. E 79 (2009) 046711.
[143] R. Carles, Semi-Classical Analysis for Nonlinear Schrödinger Equations, World Scentific, 2008.
[144] P. Gerard, P.A. Markowich, N.J. Mauser, F. Poupaud, Comm. Pure Appl. Math. 50 (1997) 321.
[145] L.-T. Cheng, H. Liu, S. Osher, Commun. Math. Sci. 1 (2003) 593.
[146] P.A. Markowich, P. Pietra, C. Pohl, H.P. Stimming, A Wigner-measure analysis of the Dufort–Fraenkel scheme for the Schrödinger equation, SIAM J. Numer. Anal. 40 (2002) 1281.
[147] E. Faou, V. Gradinaru, Ch. Lubich, SIAM J. Sci. Comput. 31 (2009) 3027.
[148] S. Jin, H. Wu, X. Yang, Commun. Math. Sci. 6 (2008) 995.
[149] S. Jin, H. Wu, X. Yang, Z. Huang, J. Comput. Phys. 229 (2010) 4869.
[150] S. Leung, J. Qian, J. Comput. Phys. 228 (2009) 2951.
[151] J. Qian, L. Ying, J. Comput. Phys. 229 (2010) 7848.
[152] G. Russo, P. Smereka, The Gaussian wave packet transform: efficient computation of the semi-classical of the Schödinger equation: part 1 — the formulation and the one dimensional case, Preprint.
[153] E. Madelung, Z. Phys. 40 (1927) 322.
[154] R. Carles, L. Gosse, Math. Models Methods Appl. Sci. 17 (2007) 1531.
[155] P. Degond, S. Gallego, F. Méhats, C. R. Math. Acad. Sci. Paris 345 (2007) 531.
[156] S. Jin, H. Liu, S. Osher, T.-H.R. Tsai, J. Comput. Phys. 205 (2005) 222.
[157] E. Grenier, Proc. Amer. Math. Soc. 126 (1998) 523.
[158] R. Carles, B. Mohammadi, ESAIM Math. Model. Numer. Anal. 45 (2011) 981.
[159] C. Besse, R. Carles, F. Méhats, An asymptotic preserving scheme based on a new formulation for NLS in the semiclassical limit. arXiv:1211.3391v1.
[160] E.A. Donley, N.R. Claussen, S.L. Cornish, J.L. Roberts, E.A. Cornell, C.E. Wieman, Nature 412 (2001) 295.
[161] W. Bao, D. Jaksch, SIAM J. Numer. Anal. 41 (2003) 1406.
[162] W. Bao, D. Jaksch, P.A. Markowich, J. Phys. B: At. Mol. Opt. Phys. 37 (2004) 329.
[163] J.R. Abo-Shaeer, C. Raman, J.M. Vogels, W. Ketterle, Science 292 (2001) 476.
[164] A. Aftalion, Q. Du, Phys. Rev. A 64 (2001) 063603.
[165] K.W. Madison, F. Chevy, W. Wohlleben, J. Dalibard, Phys. Rev. Lett. 84 (2000) 806.
[166] W. Bao, H. Wang, J. Comput. Phys. 217 (2006) 612.
[167] A.L. Fetter, Rev. Modern Phys. 81 (2009) 647.
[168] W. Bao, Q. Du, Y. Zhang, SIAM J. Appl. Math. 66 (2006) 758.
[169] W. Bao, H.-L. Li, J. Shen, SIAM J. Sci. Comput. 31 (2009) 3685.
[170] W. Bao, D. Marahrens, Q. Tang, Y. Zhang, A simple and efficient numerical method for computing the dynamics of rotating Bose–Einstein condensates via rotating Lagrangian coordinates. arXiv:cond-mat 1305.1378.
[171] P. Antonelli, D. Marahrens, C. Sparber, Discrete Contin. Dyn. Syst. Ser. A 32 (2012) 703.
[172] J.J. García-Ripoll, V.M. Pérez-García, V. Vekslerchik, Phys. Rev. E 64 (2001) 056602.
[173] J.P. Boyd, J. Comput. Phys. 103 (1992) 243.
[174] J. Shen, T. Tang, L. Wang, Spectral Methods: Algorithms, Analysis and Applications, Springer, 2011.
[175] W. Bao, Multiscale Model. Simul. 2 (2004) 210.
[176] W. Bao, Contemp. Math. 473 (2008) 1.
[177] W. Bao, C. Zheng, Commun. Comput. Phys. 2 (2007) 123.
[178] W. Bao, P.A. Markowich, C. Schmeiser, R.M. Weishäupl, Math. Models Methods Appl. Sci. 15 (2005) 767.
[179] Y. Zhang, W. Bao, H.-L. Li, Physica D 234 (2007) 49.
[180] H. Wang, J. Comput. Appl. Math. 205 (2007) 88.
[181] H. Wang, W. Xu, Comput. Phys. Comm. 182 (2011) 706.
[182] W. Bao, Y. Zhang, Methods Appl. Anal. 17 (2010) 49.
[183] W. Bao, Y. Cai, Uniform and optimal error estimates of an exponential wave integrator sine pseudospectral method for the nonlinear Schrödinger equation with wave operator. arXiv:math.NA 1305.6377.
[184] Y. Zhang, X. Dong, J. Comput. Phys. 230 (2011) 2660.
[185] S. Jin, P.A. Markowich, C. Zheng, J. Comput. Phys. 201 (2004) 376.
[186] W. Bao, F.F. Sun, G.W. Wei, J. Comput. Phys. 190 (2003) 201.
[187] W. Bao, F.F. Sun, SIAM J. Sci. Comput. 26 (2005) 1057.
[188] W. Bao, L. Yang, J. Comput. Phys. 225 (2007) 1863.
[189] Y. Zhang, W. Bao, Q. Du, SIAM J. Appl. Math. 67 (2007) 1740.
[190] W. Bao, H. Wang, P.A. Markowich, Commun. Math. Sci. 3 (2005) 57.
[191] E. Zaremba, T. Nikuni, A. Griffin, J. Low Temp. Phys. 116 (1999) 277.
[192] M. Barton-Smith, A. Debussche, L. Di Menza, Numer. Methods Partial Differential Equations 21 (4) (2005) 810.
[193] A. De Bouard, A. Debussche, Appl. Math. Optim. 54 (3) (2006) 369.
[194] A. De Bouard, A. Debussche, L. Di Menza, Monte Carlo Methods Appl. 7 (1–2) (2001) 55.
[195] A. Debussche, L. Di Menza, Physica D 162 (3–4) (2002) 131.
[196] R. Marty, Commun. Math. Sci. 4 (4) (2006) 679.
[197] M. Caliari, S. Rainer, Comput. Phys. Comm. 184 (3) (2013) 812.
[198] R.M. Caplan, Comput. Phys. Comm. 184 (4) (2013) 1250.
[199] D. Vudragovic, I. Vidanovic, A. Balaz, P. Muruganandam, S.K. Adhikari, Comput. Phys. Comm. 183 (9) (2012) 2021.